JOURNAL OF GEOPHYSICAL RESEARCH, VOL. 104, NO. D21, PAGES 26,419-26,436, NOVEMBER 20, 1999

Maintenance of high HCl/Cl_y and NO_x/NO_y in the Antarctic vortex: A chemical signature of confinement during spring

H. A. Michelsen,[1,2] C. R. Webster,[3] G. L. Manney,[3] D. C. Scott,[3] J. J. Margitan,[3]
R. D. May,[3] F. W. Irion,[3] M. R. Gunson,[3] J. M. Russell III,[4] and
C. M. Spivakovsky[5]

Abstract. Observations made in the 1994 Antarctic vortex show that Cl_y recovered completely into HCl following conversion of Cl_y reservoir species to active radicals, and NO_x constituted a 4-5 times higher fraction of NO_y inside the vortex than outside. Measurements made in October and November from the Airborne Southern Hemisphere Ozone Expedition/Measurements of the Atmospheric Effects of Stratospheric Aircraft (ASHOE/MAESA) ER-2 aircraft mission, the third Atmospheric Laboratory for Applications and Science (ATLAS-3) space shuttle mission, and the Upper Atmosphere Research Satellite (UARS) demonstrate that this unusual partitioning of Cl_y and NO_y was maintained for at least 4 weeks in the springtime vortex. In response to severe ozone loss, abundances of HCl and NO_x remained high despite temperatures low enough to reactivate Cl_y and convert NO_x to HNO_3 via heterogeneous processes. Thus, under severely ozone depleted conditions, high HCl and NO_x abundances in the vortex are maintained until the vortex breaks up or an influx of ozone-rich extravortex air is entrained into the vortex. These observations suggest that the flux of extravortex air entering the core of the lower stratospheric vortex was small or negligible above ~400 K during late spring, despite weakening of the vortex during this time period. Results of a photochemical model constrained by the measurements suggest that extravortex air entrained into the vortex during October and early November made up less than 5% of the vortex core air at 409 K. The model results also show that heterogeneous chemistry has little effect on the Cl_y and NO_y partitioning once high abundances of HCl have been attained under ozone depleted conditions, even when aerosol loading is high.

1. Introduction

Except during brief episodes that occur annually in the lower stratospheric polar regions, the majority of stratospheric inorganic chlorine (Cl_y) is partitioned into the relatively stable species HCl and $ClNO_3$ [e.g., *Dessler et al.*, 1995; *Michelsen et al.*, 1996]. When temperatures fall below ~195 K in the polar vortices during the winter and early spring, these species are rapidly converted to Cl_2 via heterogeneous reactions that proceed on or in polar stratospheric cloud (PSC) particles [e.g., *Solomon et al.*, 1986; *McElroy et al.*, 1986; *Molina et al.*, 1987; *Tolbert et al.*, 1987; *Webster et al.*, 1993; *Kawa et al.*, 1992, 1997; *Jaeglé et al.*, 1997]. Molecular chlorine is subsequently photolyzed to produce Cl atoms, which react with O_3 to produce ClO, thereby initiating a series of catalytic cycles that can lead to severe ozone loss in the polar spring [e.g., *Molina and Molina*, 1987; *deZafra et al.*, 1987, 1989; *Anderson et al.*, 1989; *Salawitch et al.*, 1990; *Toohey et al.*, 1993; *Müller et al.*, 1994].

As the polar stratosphere warms in late spring, the heterogeneous production of photo-labile chlorine ceases, and the reactive radicals Cl and ClO (ClO_x) begin to regenerate the more stable reservoir species HCl and $ClNO_3$. This recovery proceeds through a limited number of gas-phase reactions. Recovery into $ClNO_3$ and HCl occurs primarily via

(R1) $$ClO + NO_2 \rightarrow ClNO_3$$

and

(R2) $$Cl + CH_4 \rightarrow HCl + CH_3$$

with a minor contribution (≤~10%) from

(R3) $$ClO + OH \rightarrow HCl + O_2 .$$

The production rate for $ClNO_3$ depends on the availability of ClO and NO_2, whereas that of HCl relies on the availability of Cl. The relative production rates for HCl and $ClNO_3$ are therefore determined by the partitioning of ClO_x, which is controlled by the reactions

(R4) $$ClO + NO \rightarrow Cl + NO_2$$

(R5) $$Cl + O_3 \rightarrow ClO + O_2 ,$$

and the partitioning between NO and NO_2 (NO_x), which is determined predominantly by (R4) and

[1]Sandia National Laboratories, Livermore, California.
[2]Formerly at Atmospheric and Environmental Research, Inc., San Ramon, California.
[3]Jet Propulsion Laboratory, California Institute of Technology, Pasadena, California.
[4]Center for Atmospheric Sciences, Hampton University, Hampton, Virginia.
[5]Department of Earth and Planetary Sciences, Harvard University, Cambridge, Massachusetts.

Paper number 1999JD900473.
0148-0227/99/1999JD900473$09.00

(R6) $NO_2 + h\nu \rightarrow NO + O$

(R7) $NO + O_3 \rightarrow NO_2 + O_2$.

The combined influence of these seven reactions causes lower stratospheric chlorine partitioning to be highly sensitive to ozone concentrations.

Previous studies have shown that following chlorine activation during winter in the Arctic vortex and subsequent warming of the vortex during early spring, ClO and Cl initially produce predominantly $ClNO_3$ rather than HCl upon deactivation when a sufficient abundance of O_3 is available [*Webster et al.*, 1993; *Müller et al.*, 1994; *Santee et al.*, 1996; *Rex et al.*, 1997; *Becker et al.*, 1998]. *Prather and Jaffe* [1990] predicted, on the other hand, that when O_3 abundances were low, curtailment of (R5) and (R7) would lead to the partitioning of ClO_x into Cl and the partitioning of NO_x into NO, production of $ClNO_3$ would be limited by the availability of ClO and NO_2, and production rates of $ClNO_3$ would be slow compared to those for HCl. The net result should be preferential partitioning of Cl_y into HCl under ozone-depleted conditions, such as those encountered in the springtime Antarctic vortex. In confirmation of this prediction, several studies have reported observations of Cl_y partitioned predominantly into HCl in the polar vortex during austral spring [*Douglass et al.*, 1995; *Rinsland et al.*, 1996; *Santee et al.*, 1996; *Grooss et al.*, 1997; *Mickley et al.*, 1997].

In the Arctic, the initial production of peak abundances of $ClNO_3$ occurs within 2-4 weeks of the last time an air mass experienced temperatures low enough to facilitate substantial chlorine activation [*Müller et al.*, 1994; *Becker et al.*, 1998]; the subsequent redistribution of Cl_y to typical steady state values of 60-80% HCl and 20-40% $ClNO_3$ takes place on a timescale of ~2 months [*Douglass et al.*, 1995]. Chlorine partitioning in the lower stratospheric Arctic vortex is therefore generally unlikely to have approached photochemical steady state throughout most of the spring. When O_3 abundances are low (<~1 ppm), however, Cl_y partitioning is driven rapidly, within 2-3 weeks, to the steady state condition dominated by HCl [*Douglass et al.*, 1995; *Mickley et al.*, 1997; *Grooss et al.*, 1997]. Thus, unless perturbed by an influx of ozone-rich air, HCl abundances in an ozone-depleted polar vortex will remain high until the vortex breaks up.

Similar behavior is demonstrated for species comprising total reactive nitrogen (NO_y) within the vortex. Except during the polar vortex recovery period, when $ClNO_3$ concentrations can be unusually high, the majority of stratospheric NO_y is confined to NO_x and HNO_3. In the middle and upper stratosphere, the partitioning between NO_x and HNO_3 is controlled by

(R8) $OH + NO_2 + M \rightarrow HNO_3 + M$,

(R9a) $OH + HNO_3 \rightarrow H_2O + NO_3$,

(R9b) $NO_3 + h\nu \rightarrow NO_2 + O$,

(R10) $HNO_3 + h\nu \rightarrow OH + NO_2$.

In the lower stratosphere, heterogeneous processes, such as

(R11a) $NO_2 + NO_3 \rightarrow N_2O_5$

(R11b) $N_2O_5 + H_2O$ (aerosol) $\rightarrow 2HNO_3$,

can channel NO_x to HNO_3. When O_3 abundances are low, NO_x is partitioned in favor of NO, as discussed above, resulting in little formation of NO_2 and NO_3, thus limiting the production of HNO_3 via (R8) and (R11) and shifting the partitioning of NO_y toward NO_x. The partitioning between HNO_3 and NO_x is therefore extremely sensitive to ozone abundances, and entrainment of ozone-rich air into the otherwise ozone-depleted vortex will have a dramatic effect on the NO_y partitioning. In an ozone-depleted environment, small changes in the abundance of O_3 can lead to significant changes in the Cl_y and NO_y partitioning. Under these conditions, observations may be much more sensitive to such changes in the partitioning of NO_y and Cl_y than to the corresponding changes in O_3 abundance, making measurements of Cl_y and NO_y species a better diagnostic of entrainment of ozone-rich air into the vortex than direct observations of the abundance of O_3.

The "transport barrier" at the edge of the Arctic vortex has been shown to be permeable enough to allow filaments of extravortex air to mix into the core of the vortex during boreal winter and spring [*Manney et al.*, 1994, 1998; *Plumb et al.*, 1994; *Dahlberg and Bowman*, 1995; *Bird et al.*, 1997]. Although mixing has been shown to occur between extravortex air and air from the Antarctic vortex edge during the corresponding time period in the Southern Hemisphere [*Tuck et al.*, 1995a; *Waugh et al.*, 1997], entrainment of extravortex air into the core of the Antarctic vortex above ~400 K has not been observed and is thought to be limited [*Bowman*, 1993; *Manney et al.*, 1994, 1999; *Tuck et al.*, 1995a]. Below 400 K, the Antarctic polar vortex dynamics has dramatically different characteristics. This region, recently dubbed the "subvortex" [*McIntyre*, 1995], has been shown to be much more permeable than the vortex above 400 K [*Hartmann et al.*, 1989; *Tuck*, 1989; *Bowman*, 1993; *Chen*, 1994; *Manney et al.*, 1994; *McIntyre*, 1995] and susceptible to perturbations from tropospheric disturbances [*McIntyre*, 1995].

Measurements made during the Airborne Southern Hemisphere Ozone Expedition/Measurements of the Atmospheric Effects of Stratospheric Aircraft (ASHOE/MAESA) ER-2 aircraft campaign and by the Halogen Occultation Experiment (HALOE) satellite instrument demonstrate that Cl_y observed in air masses within the lower stratospheric Antarctic vortex was fully chemically activated to reactive chlorine in August and early September 1994 [*Tuck et al.*, 1995b; *Grooss et al.*, 1997; *Jaeglé et al.*, 1997; *Kawa et al.*, 1997]. By early October nearly all of Cl_y encountered in such air masses was in the form of HCl [*Grooss et al.*, 1997]. In addition, more than 50% of available NO_y was in the form of NO_x. The Atmospheric Trace Molecule Spectroscopy (ATMOS) space-shuttle instrument observed similar conditions during the third Atmospheric Laboratory for Applications and Science (ATLAS-3) shuttle mission in early November [*Rinsland et al.*, 1996], 3-4 weeks prior to the breakup of the vortex [*Manney et al.*, 1996, 1999].

We combine these remote and in situ observations from spring 1994 to show that the chemical composition of the Antarctic vortex in the lower stratosphere was established prior to the October flights of ASHOE/MAESA and concurrent observations from HALOE, and was maintained at least through the ATLAS-3 space-shuttle mission, which ended on November 12. Since the Cl_y and NO_y partitioning is highly sensitive to changes in O_3 abundance, these results demonstrate that the flux of extravortex air entering the Antarctic vortex was negligible during late spring of 1994 as the lower stratospheric vortex was starting to weaken. These results also show that low-temperature heterogeneous processes responsible for wintertime polar activation of Cl_y reservoir

species and production of HNO_3 have little effect on HCl, $ClNO_3$, NO_x, and HNO_3 abundances under ozone-depleted conditions.

2. Measurement Techniques

In situ data were obtained from the NASA ER-2 aircraft during the ASHOE/MAESA field campaign, from deployments based in Christchurch, New Zealand, in early October 1994. Concentrations of HCl, N_2O, and CH_4 were measured by the Aircraft Laser Infrared Absorption Spectrometer (ALIAS), a scanning tunable diode laser spectrometer, which uses high-resolution laser absorption in the 3-8 μm wavelength region [*Webster et al.*, 1994]. The fidelity of the measurement of [HCl] in the multi-pass cell was checked by simultaneously recording strong CH_4 lines close to the HCl absorption line used. (Throughout this paper, [X] denotes the volume mixing ratio of species X.) [ClO] was measured using resonance fluorescence detection of Cl atoms at 118.9 nm, which were generated by chemical conversion of ambient ClO to Cl by addition of NO [*Stimpfle et al.*, 1994]. [NO] was measured using chemiluminescence following reaction of ambient NO with added O_3 [*Fahey et al.*, 1993], and [NO_2] was measured by the same instrument following photolysis to NO [*Gao et al.*, 1994]. [O_3] observations were made using UV absorption [*Proffitt et al.*, 1983]. For these observations, estimated (1σ) accuracies were approximately 30% for NO_2, 15% for ClO and NO, 10% for HCl, 5% for N_2O and CH_4, and 3% for O_3.

ATMOS, a solar occultation, high-resolution Fourier transform spectrometer, flew as part of the ATLAS-3 space-shuttle mission, measuring vertical profiles of ~30 species. During this mission, which took place on November 4-12, 1994, sunrise occultations were viewing latitudes of 64.5-72.4°S, allowing observations to be made inside and outside the Antarctic vortex [*Gunson et al.*, 1996].

We have used ATMOS Version 3 retrievals from spectral filters 3, 9, and 12. Measurements used in this analysis have an estimated (1σ) accuracy of ±5% for [N_2O], [CH_4], [HCl], and [NO]; ±6% for [O_3] and [NO_2]; ±16% for [HNO_3] and [N_2O_5]; and ±20% for [$ClNO_3$] and [HNO_4]. The precision is estimated to be better than 5% for [N_2O], [CH_4], and [O_3]; 6% for [HNO_3]; 8% for [HCl]; 10% for [NO_2]; 20% for [NO]; 40% for [$ClNO_3$]; and 60% for [HNO_4] [*Abrams et al.*, 1996a]. Precision deteriorates in the lower stratosphere and upper troposphere, however, particularly for species, such as O_3, with a maximum mixing ratio in the middle stratosphere. Below ~450 K (~70 mbar), the precision for [O_3] is estimated to be 10-30% [*Abrams et al.*, 1996a; *Gunson et al.*, 1996]. [NO_y] was derived from the sum of measured [HNO_3], [NO], [NO_2], [$ClNO_3$], 2[N_2O_5], and [HNO_4] [*Michelsen et al.*, 1998a]. Comparisons of ATMOS Version 2 [NO_y] versus [N_2O] with in situ observations have demonstrated agreement to within 13% for ER-2 aircraft data [*Chang et al.*, 1996a; *Michelsen et al.*, 1999a; *Rinsland et al.*, 1999] and 15% for balloon measurements [*Kondo et al.*, 1996, 1999; *Sugita et al.*, 1998], yielding an estimated accuracy of ±15% for ATMOS [NO_y] for which the precision is estimated to be better than 10-15% in the lower stratosphere and better than 5% above ~20 km [*Michelsen et al.*, 1998a]. Similar comparisons of ATMOS Version 2 observations with ER-2 measurements have demonstrated agreement to within 13-40% for [HCl] (agreement closer to 13% was achieved when [HCl] exceeded 1 ppb), 3% for [CH_4], and 28% for [O_3] [*Chang et al.*, 1996a,b]. When air mass history is taken into account, agreement has been shown to be within 7% for [HCl], 1% for [CH_4], and 10% for [O_3] [*Michelsen et al.*, 1999a].

HALOE is a solar occultation instrument that flies on the Upper Atmosphere Research Satellite (UARS), which was launched in 1991. We used observations of [O_3], [CH_4], [NO], [NO_2], and [HCl] by HALOE (Version 19) from October 10-20, 1994. Comparisons of observations from HALOE (Version 17) and ATMOS (Version 1) indicate that HALOE is systematically lower than ATMOS by 10-20% for [HCl] [*Russell et al.*, 1996] and that the instruments agree to within 5% at pressures of 2-50 mbar (500-1500 K) for [O_3] [*Brühl et al.*, 1996], 20% at 2-20 mbar (700-1500 K) for [NO] and [NO_2] [*Gordley et al.*, 1996], and 5% at 1-100 mbar (400-1900 K) for [CH_4] [*Park et al.*, 1996]. Comparisons of HALOE (Version 17) and ER-2 [O_3] observations show agreement to within 10% at ER-2 cruise altitudes (470-500 K) [*Grose et al.*, 1997]. As with the ATMOS observations, however, uncertainties for HALOE observations increase below ~450 K, and differences between HALOE and ER-2 [O_3] measurements in the lower stratosphere have been observed to be as high as 50% [*Grose et al.*, 1997].

3. Model Description

We used an updated version of the Harvard photochemical code to simulate the chemistry that occurred in the stratosphere during polar spring [see *Michelsen et al.*, 1999b]. Values of [O_3], [CH_4], [H_2O], [CO], [C_2H_6], and aerosol surface area input into the model were based on measurements from the ER-2, ATMOS, HALOE, and the Stratospheric Aerosol and Gas Experiment II (SAGE II) instrument. Kinetic parameters for the gas-phase reactions were based on recommended values [*DeMore et al.*, 1997] with modifications to the rates of $ClO+OH \rightarrow HCl+O_2$ (R3) [*Lipson et al.*, 1997], $Cl+CH_4 \rightarrow HCl+CH_3$ (R2) [*Michelsen et al.*, 1996], $OH+HCl \rightarrow Cl+H_2O$ [*Michelsen et al.*, 1996; *Battin-Leclerc et al.*, 1999], $OH+HNO_3 \rightarrow NO_3+H_2O$ (R9a) [*Brown et al.*, 1999a], $OH+NO_2+M \rightarrow HNO_3+M$ (R8) [*Brown et al.*, 1999b], and $O(^2P)+NO_2 \rightarrow NO+O_2$ [*Gierczak et al.*, 1999]. The net impact of the former three modifications on the modeled partitioning of stratospheric Cl_y has been described previously [*Michelsen et al.*, 1996], as has the effect of the latter three modifications on modeled stratospheric NO_y partitioning [*Gao et al.*, 1999; *Osterman et al.*, 1999]. Parameterizations for the reactive uptake coefficients for relevant heterogeneous reactions were derived from recent laboratory studies [*Abbatt*, 1995; *Donaldson et al.*, 1997; *Tabazadeh et al.*, 1997; *Hanson*, 1998]. The model can be run with the assumption of photochemical steady state, such that the net photochemical production of short-lived species balances net photochemical loss over a 24-hour period. Alternatively, the model can be run in a relaxation mode in which species concentrations evolve with time from the initial conditions.

4. Analysis Methodology

Data from ATMOS/ATLAS-3 sunrise and HALOE sunset profiles and from the ascent, descent, and dive portions of the ASHOE/MAESA flights on October 10 and 13 were divided into three categories, which were used to distinguish between air encountered inside, outside, and within the edge of the Antarctic vortex. The distinction between these regions was based predominantly on the potential vorticity (PV) derived from U. K. Meteorological Office (UKMO)- and National

Centers for Environmental Prediction (NCEP)-analyzed winds and temperatures [e.g., *Manney et al.*, 1996; *Nash et al.*, 1996; *Sobel et al.*, 1997]. To facilitate the sorting of data acquired over a wide range of altitude, PV was scaled to yield similar values at different theta levels throughout the stratosphere by normalizing to a standard value of the static stability [*Dunkerton and Delisi*, 1986; *Manney and Zurek*, 1993]. Above 400 K (approximately corresponding to an altitude of 15 km and pressure of 100 mbar), observations were classified as extravortex data if they fell in the lowest 10% of the range in absolute value of scaled potential vorticity (sPV) [*Manney et al.*, 1994, 1996] and were identified as vortex data if they fell in the highest 30% of this range, which reflects the higher variability in PV in the vortex. (The highest and lowest sPV values were determined separately for ATMOS and HALOE; the ER-2 data were sorted according to the sPV bins determined for the ATMOS data, which were in good agreement with the HALOE limits at the ER-2 altitudes.) The flow of air below 400 K makes the distinction between subvortex, extravortex, and edge air difficult or impossible to determine; we thus restrict our discussion to levels above 400 K. Edge data were identified with points within the altitude-dependent half-width centered around the midpoint in sPV between the mean vortex and extravortex values, i.e., at each altitude, data were considered to be in the vortex edge if they fell within the range given by

$$\frac{(\langle sPV_{Xvortex}\rangle + \langle sPV_{vortex}\rangle)}{2} \pm \frac{(\langle sPV_{Xvortex}\rangle - \langle sPV_{vortex}\rangle)}{4}, \quad (1)$$

where $\langle sPV_{Xvortex}\rangle$ represents the mean altitude-dependent value of sPV outside the vortex, and $\langle sPV_{vortex}\rangle$ represents the mean value inside the vortex. A detailed analysis of the meteorological conditions during this time period, provided by *Manney et al.* [1996, 1999], demonstrates that the location and width (as a function of sPV) of the region of strong sPV gradients demarcating the vortex edge is consistent with these definitions of vortex, edge, and extravortex regions. Since the vortex was tilted, a number of ATMOS occultations were located inside the vortex at some altitudes and outside the vortex at others. These occultations were excluded from this analysis except for the one or two measurements from each mixed profile that were made within the vortex edge region. ATMOS, HALOE, and ER-2 observations significantly perturbed by tropical or subtropical (low-PV) air were also excluded. For ATMOS and HALOE data, averages were derived by interpolation to a potential temperature grid and were weighted by the experimental uncertainty estimated for each retrieval. For the ER-2 data, averages were derived within 20 K potential temperature bins. Since, in most cases presented here, random error dominates the experimental uncertainty, error bars represent the (1σ) standard deviation of the mean except where noted otherwise.

Plate 1 shows vertical profiles of $[N_2O]$, $[CH_4]$, and $[O_3]$, color coded by region. Despite the wide range of values measured for these species at each potential temperature, the ER-2, ATMOS, and HALOE data demonstrate excellent agreement when the distinction between the origin of the air mass is taken into account. Comparisons between the measurements are summarized in Figure 1. Mean values of $[N_2O]$ and $[CH_4]$ measured from each platform differ by ≤8% at altitudes of 15-20 km, i.e., between 400 and 500 K. Except for a discrepancy of 35% near 410 K, ATMOS and ER-2 $[NO_y]$ agree to within 14% inside and outside the vortex. For HCl above 450 K, ATMOS demonstrates a high bias, relative to HALOE observations, of 10-15%, which is consistent with previous comparisons [*Russell et al.*, 1996]. ATMOS [HCl] agrees with ER-2 values to ±9% outside (19% inside) the vortex. These differences are less than the standard deviation calculated from the mean of the ER-2, ATMOS, or HALOE measurements and are well within the total error estimated for each measurement. Outside the vortex, $[O_3]$ measurements demonstrate agreement to within 8% between ATMOS and HALOE and to within 10% between ATMOS and the ER-2 (except for a discrepancy of 35% near 410 K). Similarly good agreement is observed when $[CH_4]$, $[O_3]$, $[NO_y]$, and [HCl] are plotted relative to $[N_2O]$, as shown in Plate 2. Although differences in $[O_3]$ observations inside the vortex are as much as 50% between ATMOS and the ER-2 and up to 75% between HALOE and ATMOS, these differences are comparable to the standard deviation calculated for the vortex observations. These large percent differences reflect small absolute differences in mixing ratio, since $[O_3]$ was severely depleted inside the vortex. In addition, there was a strong horizontal gradient in ozone inside the vortex, such that data recorded deep in the vortex core would have yielded lower values of $[O_3]$ than data obtained closer to the vortex edge. The differences between $[O_3]$ observations may partially reflect how deep within the vortex core the data were obtained. Large differences below 400 K are related to mixing of subvortex with extravortex air during October, whereas differences above 400 K inside the vortex are unlikely to have been caused by influx of extravortex air during October, as is discussed in detail below.

Since ER-2 observations of $[NO_2]$ were unavailable in vortex air masses, values were inferred by multiplying the modeled ratio of $[NO_2]$:[NO] by in situ measurements of [NO] within these air masses. Applying this method to extravortex air masses in which in situ $[NO_2]$ measurements were available reproduced the measured values to within 60% at latitudes corresponding to those at which the vortex measurements were made. NO_2 is estimated to be a small fraction (~15%) of NO_x inside the vortex, and an uncertainty of 60% in $[NO_2]$ translates into an uncertainty of <10% in $[NO_x]$. The value of $[NO_y]$ inferred from the ATMOS observations is within 4% of the value measured by HALOE.

In situ measurements of $[ClNO_3]$ were not made during ASHOE/MAESA; values were inferred from in situ observations of [ClO] and $[NO_2]$ based on the steady state relation [e.g., *Kawa et al.*, 1992; *Stimpfle et al.*, 1994]

$$[ClNO_3]_{ss} = k_{ClO+NO2+M}[ClO][NO_2]\rho / J_{ClNO3}, \quad (2)$$

where $k_{ClO+NO2+M}$ represents the rate constant (cm^3 $molecule^{-1}$ s^{-1}) [*DeMore et al.*, 1997] for

$$(R12) \qquad ClO + NO_2 + M \rightarrow ClNO_3 + M,$$

ρ (molecule cm^{-3}) is the density of third-body partner M (i.e., air), and J_{ClNO3} (s^{-1}) is the photolysis rate of $ClNO_3$.

Values for Cl_y were inferred from measured $[N_2O]$ and $[CH_4]$, as shown by the dashed line in Plate 2d [*Woodbridge et al.*, 1995]. This relation, which was derived from aircraft data from the lower stratosphere, is not valid at higher altitudes. For values of $[N_2O]$ less than 125 ppb, we used the relation (solid line in Plate 2d)

$$[Cl_y] = (3.5764\times10^{-9}) - 0.0043843[N_2O] - (2.1448\times10^{-4})[N_2O]^2 \quad (3)$$

derived from middle and upper stratospheric ATMOS observations of [HCl] and $[ClNO_3]$, Millimeter-wave Atmos-

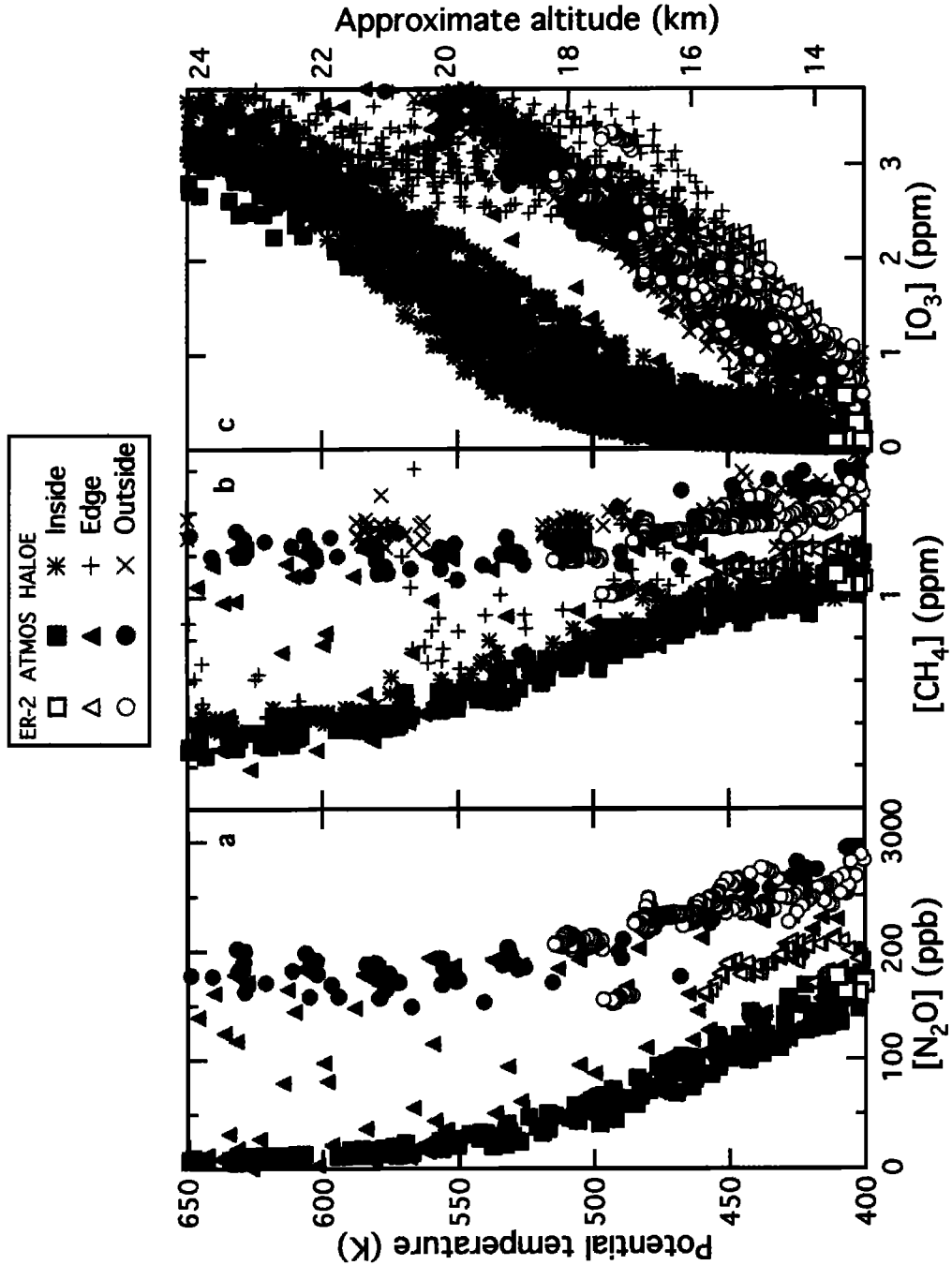

Plate 1. Vertical profiles of measured mixing ratios of (a) N_2O, (b) CH_4, and (c) O_3 relative to potential temperature. ER-2, ATMOS, and HALOE observations are shown for air masses encountered inside the vortex, outside the vortex, and in the vortex-edge region, as indicated by the legend. ER-2 data are from the ASHOE/MAESA mission (October 10 and 13, 1994), ATMOS data are from the ATLAS-3 mission (November 4-12, 1994), and HALOE data are from the UARS archive (October 10-20, 1994). The approximate altitude, with respect to extravortex temperatures and pressures, is shown for reference.

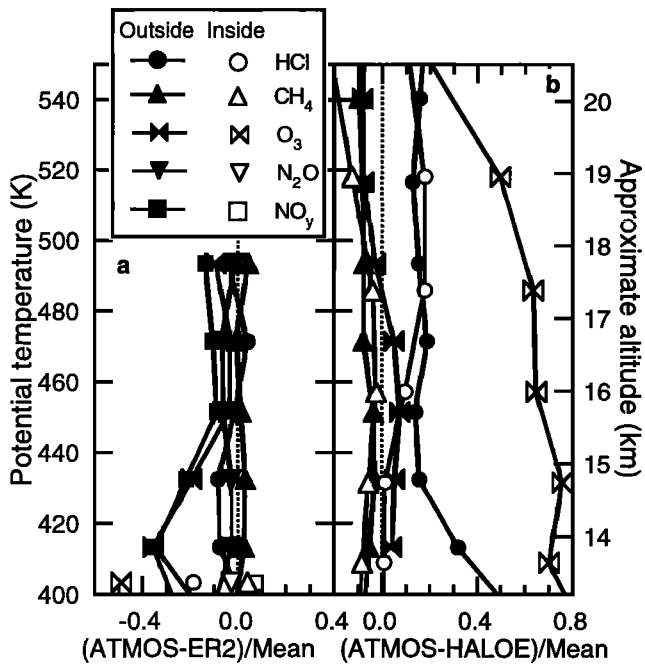

Figure 1. Differences between mean values from ATMOS and mean values from (a) ER-2 and (b) HALOE measurements relative to potential temperature. Mean values were derived separately for vortex and extravortex observations from ATMOS (November 4-12, 1994), the ER-2 (October 10 and 13, 1994), and HALOE (October 10-20, 1994), as indicated by the legend. The approximate altitude, relative to extravortex temperatures and pressures, is shown for reference.

pheric Sounder (MAS) observations of [ClO], and model estimates of [HOCl] [*Michelsen et al.*, 1996; *Zander et al.*, 1996]. Since $[N_2O]$ is not measured by HALOE, we inferred $[N_2O]$ from HALOE observations of $[CH_4]$ using the mean correlations given by ATMOS observations during this time period shown in Plate 2a. $[Cl_y]$ was then inferred for HALOE observations as described above. $[NO_y]$ was similarly inferred from HALOE observations of $[CH_4]$ based on mean correlations given by ATMOS observations. $[Br_y]$ was derived from measured values of $[CCl_3F]$ [*Wamsley et al.*, 1998].

5. Results and Discussion

5.1. Tracer Distributions Inside and Outside the Vortex

Plates 1a and 1b show that, for a given altitude, values of $[N_2O]$ and $[CH_4]$ were lower inside than outside the vortex. $[N_2O]$ and $[CH_4]$ decrease with increasing altitude, and the difference observed is attributable to descent within the vortex [e.g., *Abrams et al.*, 1996b]. $[O_3]$ is similarly lower inside the vortex than outside, as shown in Plate 1c, but the explanation for the difference is not as straightforward. Since the mixing ratio of O_3 increases with increasing altitude in the lower stratosphere, moderate descent at altitudes below the maximum in mixing ratio (at ~30 km) will lead to an enhancement in $[O_3]$ in the vortex. Although descent of air from the upper stratosphere and mesosphere, where $[O_3]$ is low, could lead to lower values of $[O_3]$ in the vortex, low $[O_3]$ in the lower stratospheric vortex is predominantly attributable to chemical depletion of $[O_3]$ by low-temperature heterogeneous processes that occur during the winter [e.g., *Solomon et al.*, 1986; *McElroy et al.*, 1986; *Molina et al.*, 1987; *Molina and Molina*, 1987; *Tolbert et al.*, 1987; *deZafra et al.*, 1987, 1989; *Anderson et al.*, 1989; *Salawitch et al.*, 1990; *Kawa et al.*, 1992, 1997; *Toohey et al.*, 1993; *Webster et al.*, 1993; *Müller et al.*, 1994; *Jaeglé et al.*, 1997].

Additional information about the reasons for differences between long-lived trace species abundances in vortex and extravortex air can be obtained by examining the tracer correlations. Plates 2a-2c illustrate the large differences in such correlations that are commonly observed between vortex and extravortex air in the late spring in both hemispheres [e.g., *Kawa et al.*, 1992; *Mickley et al.*, 1997; *Waugh et al.*, 1997; *Michelsen et al.*, 1998a,b, 1999a; *Sugita et al.*, 1998; *Kondo et al.*, 1999; *Manney et al.*, 1999; *Rex et al.*, 1999; *Rinsland et al.*, 1999; R. A. Plumb et al., The effects of mixing on tracer relationships in the polar vortices, submitted to *Journal of Geophysical Research*, 1999 (hereinafter referred to as submitted paper)]. The extravortex correlations are consistent with correlations derived previously from ATMOS extravortex/ extratropics observations (solid black lines) [*Michelsen et al.*, 1998a,b]; the small deviations from the canonical extravortex correlations apparent for $[CH_4]$:$[N_2O]$ (Plate 2a) and the large deviations for $[O_3]$:$[N_2O]$ (Plate 2c) at $[N_2O]$ values of 100-200 ppb are attributable to recent transport of unmixed low-latitude (tropical or subtropical) air to high latitudes in the middle stratosphere [*Manney et al.*, 1996, 1999].

The differences between the vortex and extravortex $[O_3]$:$[N_2O]$ correlations (Plate 2c) stem in large part from ozone destruction within the vortex, which is consistent with the differences apparent between the vortex and extravortex vertical profiles. Lower values of $[O_3]$ relative to $[N_2O]$ in the vortex can also be explained, in part, by descent of air from altitudes above the maximum in the vertical profile. If descended air is mixed with air that originates from lower altitudes, dramatic deviations from the original correlation can result, since the canonical $[O_3]$:$[N_2O]$ correlation is nonlinear [e.g., *Waugh et al.*, 1997]. Distinguishing between chemical and dynamical effects on the $[O_3]$:$[N_2O]$ vortex correlation is difficult under these circumstances. Similar ambiguities are encountered in the analysis of the vortex $[NO_y]$:$[N_2O]$ correlation (Plate 2b), which is influenced by denitrification by PSC-particle sedimentation and descent from altitudes above a maximum in $[NO_y]$, followed by mixing with lower altitude air.

The abundance of CH_4 in the vortex, in contrast, is not susceptible to significant photochemical modification during the winter. Differences between the vortex and extravortex $[CH_4]$:$[N_2O]$ correlations in Plate 2a can thus be fully attributed to mixing between air masses that originate at different altitudes following descent within the vortex [e.g., *Waugh et al.*, 1997; *Michelsen et al.*, 1998b; *Kondo et al.*, 1999; *Manney et al.*, 1999; *Rex et al.*, 1999]. The separation between the $[CH_4]$:$[N_2O]$ correlations shown here is significantly smaller than observed in the springtime Arctic vortex [*Michelsen et al.*, 1998b, 1999a; *Herman et al.*, 1998; *Kondo et al.*, 1999; R. A. Plumb et al., submitted paper, 1999; *Rex et al.*, 1999]. The tracer distributions observed in the 1993 springtime Arctic vortex have been shown to be most consistent with a substantial amount of entrainment of extravortex air into the vortex significantly prior to the break-up of the vortex [*Manney et al.*, 1999; R. A. Plumb et al., submitted paper, 1999], whereas the correlations observed in

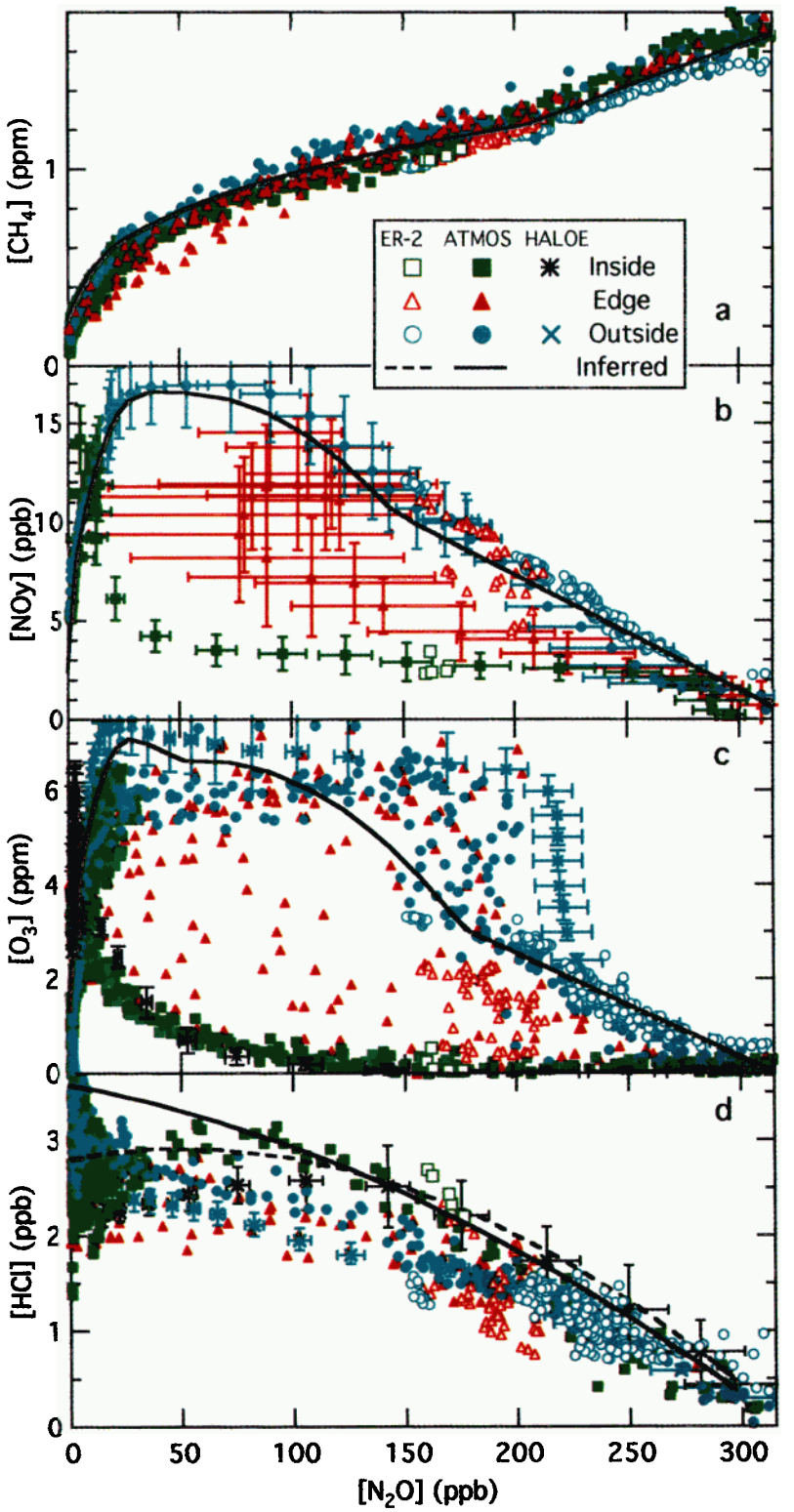

Plate 2. Correlations of measured (a) $[CH_4]$, (b) $[NO_y]$, (c) $[O_3]$, and (d) [HCl] relative to $[N_2O]$. ER-2 (October 10 and 13, 1994), HALOE (October 10-20, 1994), and ATMOS (November 4-12, 1994) observations were made inside the vortex, outside the vortex, and in the vortex-edge region, as indicated by the legend. Correlations derived from northern midlatitude observations are indicated by the solid lines in Plates 2a, 2b, and 2c, and $[Cl_y]$ inferred based on relations derived from ER-2 measurements (dashed line) and ATMOS data (solid line) are shown in Plate 2d. HALOE (c) $[O_3]$ and (d) [HCl] are plotted against $[N_2O]$ inferred from measured $[CH_4]$ based on the vortex and extravortex averages of the ATMOS correlations shown in Plate 2a.

the 1994 springtime Antarctic vortex are more consistent with a small flux of air entering the vortex throughout the winter [R. A. Plumb et al., submitted paper, 1999]. These results support previous suggestions that less extravortex air mixes into the core of the vortex in the Antarctic than in the Arctic [*Manney et al.*, 1994, 1999; *Plumb et al.*, 1994; *Dahlberg and Bowman*, 1995; *Tuck et al.*, 1995a]. Nevertheless, since the curvature of the $[O_3]$:$[N_2O]$ and $[NO_y]$:$[N_2O]$ correlations is more severe than that of $[CH_4]$:$[N_2O]$, even the relatively small amount of air mixed into the vortex indicated by the plot in Plate 2a may contribute nonnegligibly to the deviations between vortex and extravortex correlations of $[O_3]$ and $[NO_y]$ relative to $[N_2O]$ shown in Plates 2b and 2c [*Waugh et al.*, 1997; *Michelsen et al.*, 1998a; *Kondo et al.*, 1999; *Manney et al.*, 1999].

5.2. Tracer Distributions and Mixing in the Edge

The vortex edge provides a region where mixing of vortex and extravortex air can take place. In addition, independent descent of air occurs within the vortex edge itself [*Schoeberl et al.*, 1992; *Manney et al.*, 1994, 1999], which is consistent with values of $[O_3]$ in a portion of the edge that exceed those measured in extravortex air (Plate 1c) and values of $[N_2O]$ (Plate 1a) and $[CH_4]$ (Plate 1b) in the edge that are lower than those measured inside the vortex.

The vortex-edge correlations are not compact, which is consistent with slow isentropic mixing within the edge relative to the rate of influx of vortex or extravortex air into this region [*Plumb and Ko*, 1992]. In addition, the $[CH_4]$:$[N_2O]$ edge correlation has points that lie well outside the range defined by the vortex and extravortex values. There are two possible mechanisms that could lead to this observation. (1) Air that descends within the vortex may mix with extravortex air (more thoroughly than inside the vortex) via this collar region surrounding the vortex core. (2) Air within the vortex edge may descend independently of the vortex core (as suggested by the $[O_3]$ and $[CH_4]$ vertical profiles) and mix with lower altitude air. Previous studies have shown that air descends more rapidly at the edge than in the core of the vortex in the Antarctic spring [*Schoeberl et al.*, 1992; *Manney et al.*, 1994, 1999]. Other studies have demonstrated that horizontal mixing between vortex and extravortex air may take place within this region but appears not to occur in the vortex interior [*Bowman*, 1993; *Manney et al.*, 1994; *Eluszkiewicz et al.*, 1995; *Tuck et al.*, 1995a; *Waugh et al.*, 1997]. This collection of results from previous work indicates that the distinction of the vortex edge correlation is likely attributable to a combination of the two mechanisms proposed, a conclusion confirmed by a recent study of polar vortex dynamics relevant to this time period [*Manney et al.*, 1999].

5.3. Cl_y and NO_y Partitioning Inside and Outside the Vortex

Regardless of the dynamical mechanisms responsible for separating the correlations of long-lived tracers, these processes do not appear to account for the differences between the vortex, extravortex, and edge regions in the corresponding [HCl]:$[N_2O]$ correlations shown in Plate 2d. Observations show that relative to $[N_2O]$, [HCl] was generally higher inside the vortex than outside and higher outside the vortex than in the vortex edge region. Between 400 and 500 K inside the vortex, Cl_y was almost exclusively in the form of HCl in October and November, as demonstrated by the consistency of measured [HCl] with inferred $[Cl_y]$ in Plate 2d and by the altitude dependence of [HCl]/$[Cl_y]$ in Plate 3a; [HCl] made up ~70% of $[Cl_y]$ outside the vortex and ~60% at the vortex edge. Plate 3b shows that $[NO_x]$ similarly constituted a significantly higher percentage of $[NO_y]$ inside the vortex than outside or in the vortex edge region.

Plate 4a shows mean values of remote and in situ measurements of [HCl] from inside and outside the vortex, and Plate 4b displays corresponding observations of $[ClNO_3]$ from ATMOS and values inferred from ER-2 data (described above). The data agree well, despite the 1 month time difference between the observations by ATMOS and those by ALIAS and HALOE. The lines in Plate 4 represent results of photochemical model simulations assuming steady state conditions for October 11 (dashed) and November 7 (solid). The model was constrained by the mean of the measured abundances of N_2O (Plate 1a), CH_4 (Plate 1b), O_3 (Plate 1c), NO_y, and H_2O. $[Cl_y]$ was inferred from measured $[N_2O]$ and $[CH_4]$. A latitude of ~69°S and albedo of 0.8 were assumed for most of the calculations shown, except for the October extravortex case below 488 K for which a latitude of 48°S and albedo of 0.2 were assumed for better consistency with the ER-2 observations. Given these constraints, the model does a good job of reproducing the measurements.

Model estimates of $[HNO_3]$ and $[NO_x]$ yield excellent agreement with observations at all altitudes inside and outside the vortex (Plates 5a and 5b). The difference between ER-2 or HALOE and ATMOS measurements of vortex $[NO_x]$ results from the change in solar illumination at high latitudes during the month separating the observations, as demonstrated by the model results for October (dashed) in comparison to those for November (solid).

5.4. Cl_y and NO_y Partitioning in the Vortex Edge

Despite the dynamical activity at the vortex edge, the steady state model approximately reproduces values of [HCl] (Plate 4c), $[ClNO_3]$ (Plate 4d), $[HNO_3]$ (Plate 5c), and $[NO_x]$ (Plate 5d) measured during November in this region. Since the range in source gas concentrations in the edge span those observed inside and outside the vortex, we have added the model results constrained by vortex (green) and extravortex (blue) source gas abundances to these figures to represent the expected variability. The red line is the result of the calculation constrained by average edge values.

The most serious disagreement between the model results and the measurements occurs for values of $[ClNO_3]$ inferred from in situ observations of [ClO] and $[NO_2]$, which are 2-4 times larger than steady state model predictions for October (Plate 4d). A similar difference is observed between the inferred $[ClNO_3]$ and values measured by ATMOS a month later. One possible explanation for the apparent difference between inferred $[ClNO_3]$ and other measured and modeled values is that the approximation used to infer steady state values of $[ClNO_3]$, equation (2), may break down under conditions observed in the vortex edge. Since the vortex was not symmetric about the pole during October [*Manney et al.*, 1999], and air within the edge periodically made excursions from 50 to 70°S [*Pierce et al.*, 1997], a breakdown in the validity of (2) could be caused by variability in the solar conditions encountered by air masses circulating in the vortex edge [*Kawa et al.*, 1992]. Photolysis rates for $ClNO_3$ are calculated to have been ~50% larger at 50°S than at 70°S, where the in situ edge measurements were made, which would lead to a reduction by ~35% in

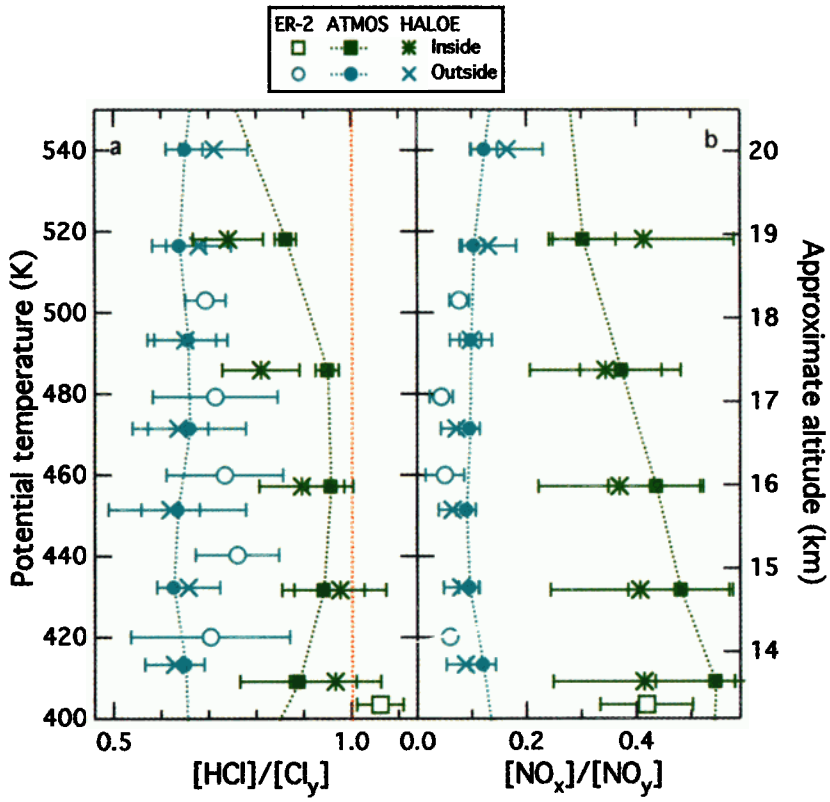

Plate 3. Vertical profiles of (a) the fraction of Cl_y in HCl and (b) the fraction of NO_y in NO_x relative to potential temperature. Mean values are displayed for data from inside the vortex, outside the vortex, or in the vortex-edge region. Averages were derived from observations from ATMOS (November 4-12, 1994), ALIAS and NOAA ER-2 instruments (October 10 and 13, 1994), and HALOE (October 10-20, 1994). Error bars represent the (1σ) standard deviation of the mean.

inferred [$ClNO_3$] if these values were used in (2). Accounting for excursions to lower latitudes would also lead to a decrease in modeled [$ClNO_3$], however, and therefore would not significantly reduce the discrepancy between modeled and measured values. Although the sum of [HCl], [ClO], and [$ClNO_3$] inferred from the ER-2 observations in the edge exceeds values of [Cl_y] estimated for these air masses by 5-31%, this discrepancy is within the combined experimental uncertainties.

The disagreement between the modeled and measured [$ClNO_3$] and the inferred values may indicate that the chlorine partitioning within the edge was not in photochemical steady state in early October but had nearly reached steady state by early November. Previous studies have noted higher values of [$ClNO_3$] at the vortex edge than in either vortex or extravortex air masses in both the Arctic [*Toon et al.*, 1992; *Blom et al.*, 1995; *Chipperfield et al.*, 1995; *Geller et al.*, 1995] and Antarctic [*Farmer et al.*, 1987; *Toon et al.*, 1989; *Roche et al.*, 1994; *Rinsland et al.*, 1996; *Schoeberl et al.*, 1996]. Modeling studies have demonstrated that, in the Arctic, high [$ClNO_3$] in the edge or "collar" region can be attributed to slow recovery of photochemically perturbed air masses to steady state conditions [*Chipperfield et al.*, 1997]. If activated chlorine were mixed into the vortex edge from the vortex interior in late winter in the Antarctic, deactivation would likely have produced high values of [$ClNO_3$] (such as those inferred from the ER-2 observations), since [O_3] was relatively high in the edge region. Under these conditions, which are similar to conditions often encountered in the springtime Arctic vortex, recovery to steady state values of [HCl] and [$ClNO_3$] would have required a number of weeks [*Douglass et al.*, 1995]. Mixing of vortex air (with high values of [HCl] relative to those of [$ClNO_3$]) into the vortex edge may have accelerated this process. By early November, [$ClNO_3$], although much more consistent with the steady state prediction, was still higher in the edge than inside the vortex because of the higher abundance of O_3 in the edge, whereas values of [$ClNO_3$] were larger in the edge than outside the vortex because [Cl_y] was significantly larger in the edge (a consequence of descent from higher altitudes). Thus [$ClNO_3$] can be highest in the edge at a particular altitude even as the Cl_y partitioning in the edge approaches steady state values.

Manney et al. [1999] have demonstrated that a distinct maximum in [HNO_3] was also apparent at the vortex edge during the 1994 austral spring, as shown in Plate 5c. Such a maximum in [HNO_3] at the edge of the Antarctic and Arctic vortices has been reported previously [*Toon et al.*, 1992; *Roche et al.*, 1994; *Blom et al.*, 1995; *Santee et al.*, 1999] and, similarly to the peak in [$ClNO_3$] at the vortex edge, is attributable to a combination of dynamical and chemical effects. Air descended from higher altitudes in the edge is enriched in NO_y relative to the extravortex air. Although vortex air may be similarly enriched in NO_y, dehydration depletes NO_y relative to the vortex edge. In addition, the percentage of NO_y in HNO_3 is decreased by a reduction in the rate of (R8) in the absence of O_3 inside the vortex.

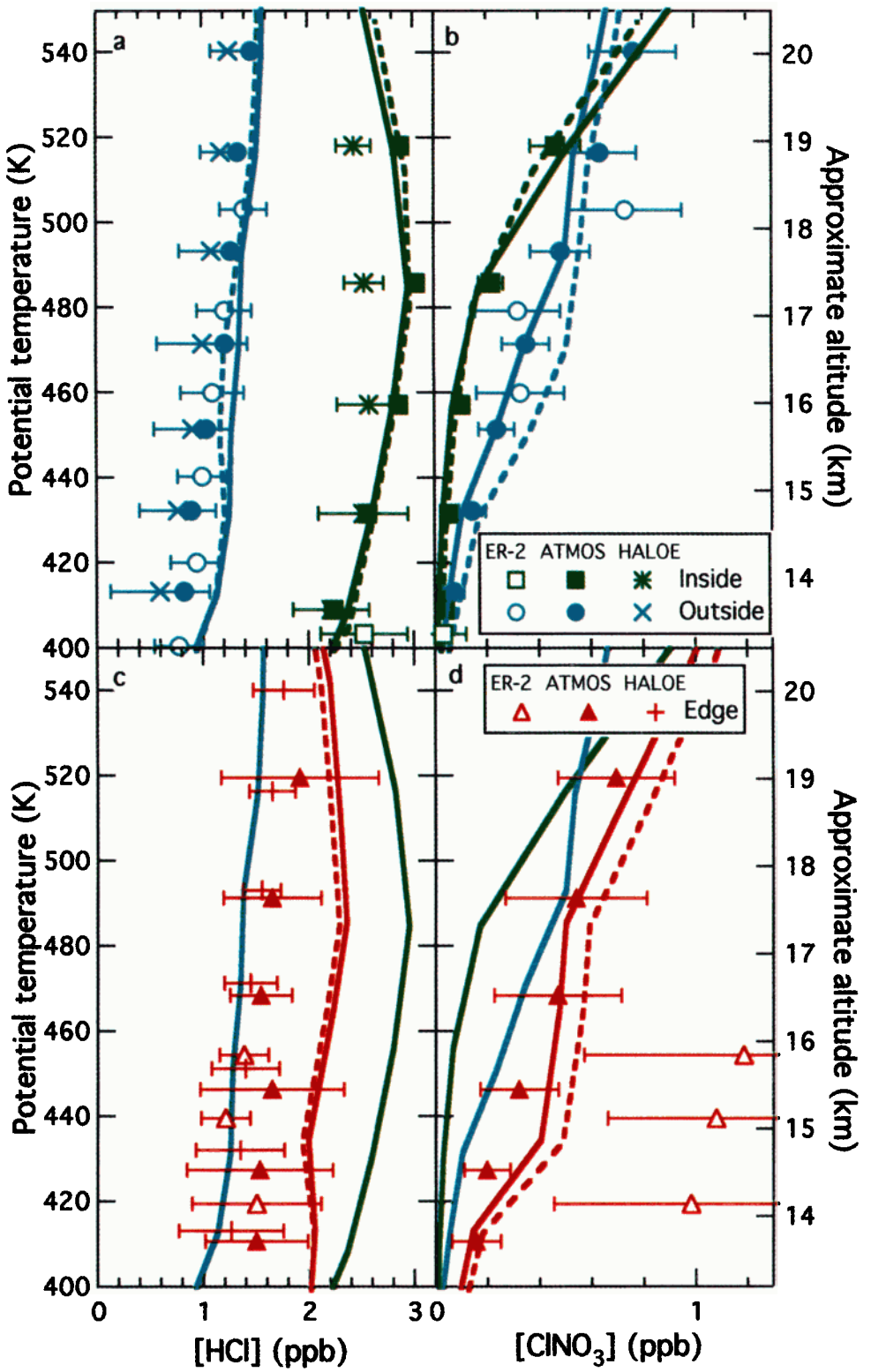

Plate 4. Vertical profiles of (a, c) HCl and (b, d) $ClNO_3$ mixing ratios relative to potential temperature. Mean values are displayed for data from (a, b) inside the vortex and outside the vortex and (c, d) in the vortex-edge region. Averages were derived from observations from ATMOS (November 4-12, 1994), ALIAS (October 10 and 13, 1994), and HALOE (October 10-20, 1994). ER-2 [$ClNO_3$] was inferred from simultaneous observations of [ClO] from the Harvard instrument and [NO_2] from the NOAA instrument. For HCl, error bars represent the (1σ) standard deviation of the mean; for $ClNO_3$, error bars represent the combined (1σ) accuracy and precision. The lines show the results of a photochemical steady state model assuming solar conditions for October (dashed) and November (solid).

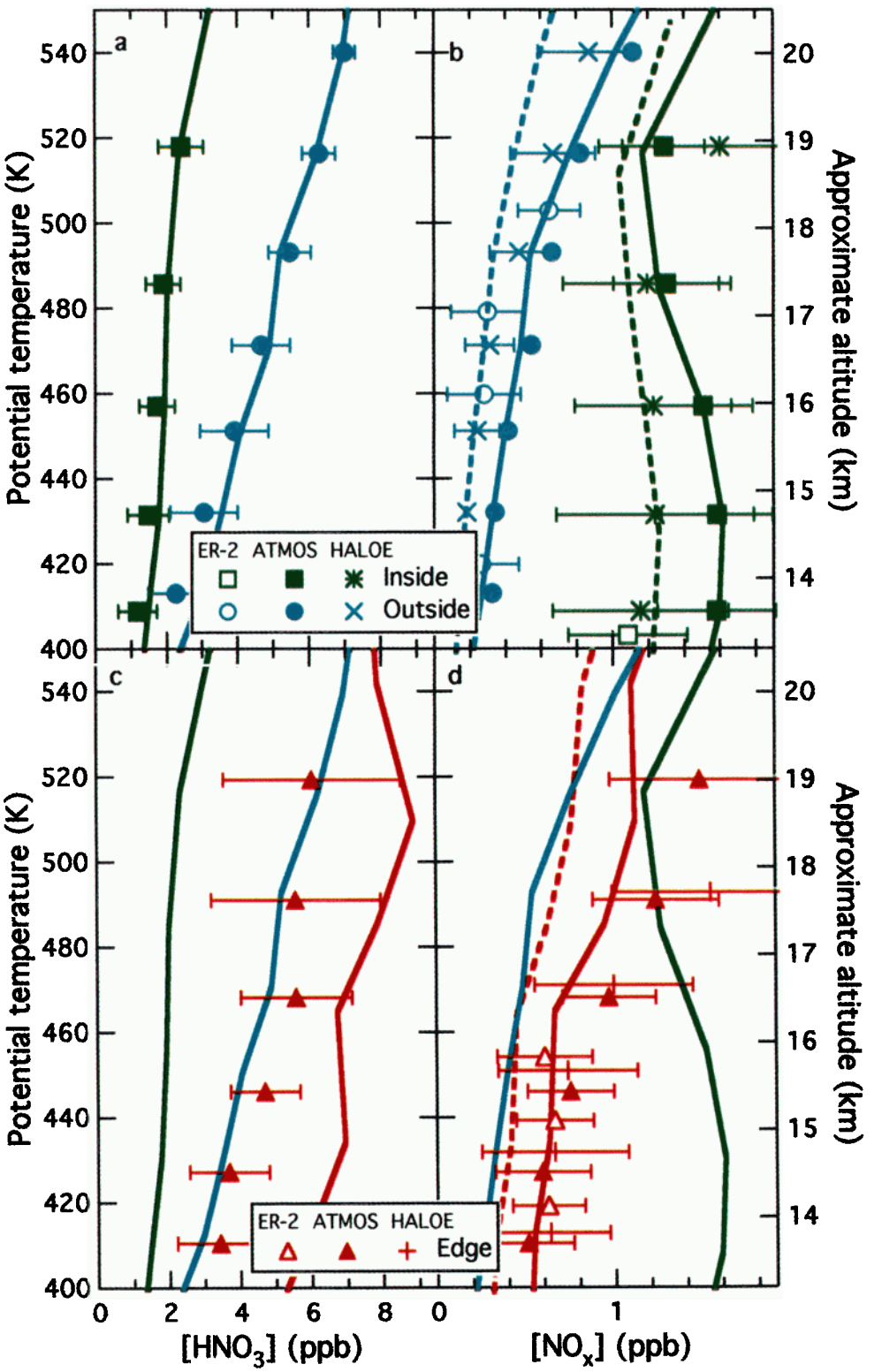

Plate 5. Vertical profiles of (a, c) HNO_3 and (b, d) NO_x mixing ratios relative to potential temperature. Mean values are displayed for data from (a, b) inside the vortex and outside the vortex and (c, d) in the vortex-edge region. Averages were derived from observations from ATMOS (November 4-12, 1994), the NOAA ER-2 instrument (October 10 and 13, 1994), and HALOE (October 10-20, 1994). ER-2 vortex $[NO_2]$ was inferred from observations of [NO] and model estimates of the $[NO_2]/[NO]$ ratio. Error bars represent the (1σ) standard deviation of the mean. The lines show the results of a photochemical steady state model assuming solar conditions for October (dashed) and November (solid).

5.5. Cl_y and NO_y Partitioning and Isolation of Vortex Air

As demonstrated in Plates 2d and 3a, HCl accounted for more than 90% of the available inorganic chlorine between 400 and 500 K inside the Antarctic vortex in October and November 1994. Plate 3b shows that NO_x made up at least 40% of NO_y at these levels inside the vortex. Good agreement with steady state predictions for the abundances of these species, shown in Plates 4 and 5, confirms that steady state conditions were attained prior to the second week of October and were maintained for at least 1 month.

Had extravortex air mixed into the vortex during this time period, perturbations to these species distributions would have been expected. To test the sensitivity of the Cl_y and NO_y partitioning to entrainment of extravortex air into the vortex, we performed a time-dependent model calculation assuming that edge air mixed into the vortex core. Plate 6 shows the evolution of (a) NO_y species, HNO_3, NO_x, and $ClNO_3$, and (b) Cl_y species, HCl and $ClNO_3$, as a function of time following the last hypothetical PSC event in which all Cl_y was converted to active radicals and all NO_y was converted to HNO_3. The calculation was performed for the 409 K surface based on abundances of O_3 (0.128 ppm), CH_4 (1.10 ppm), H_2O (2.87 ppm), and N_2O (160 ppb) measured inside the vortex with constant solar conditions assuming a latitude of 69°S for October 11 with an albedo of 0.8. The model was initialized on day 0 with all Cl_y (2.38 ppb) as active chlorine and all NO_y (2.92 ppb) as HNO_3. Within the first 1-2 weeks, more than 90% of Cl_y was in HCl, and HNO_3 lost more than 40% of NO_y to

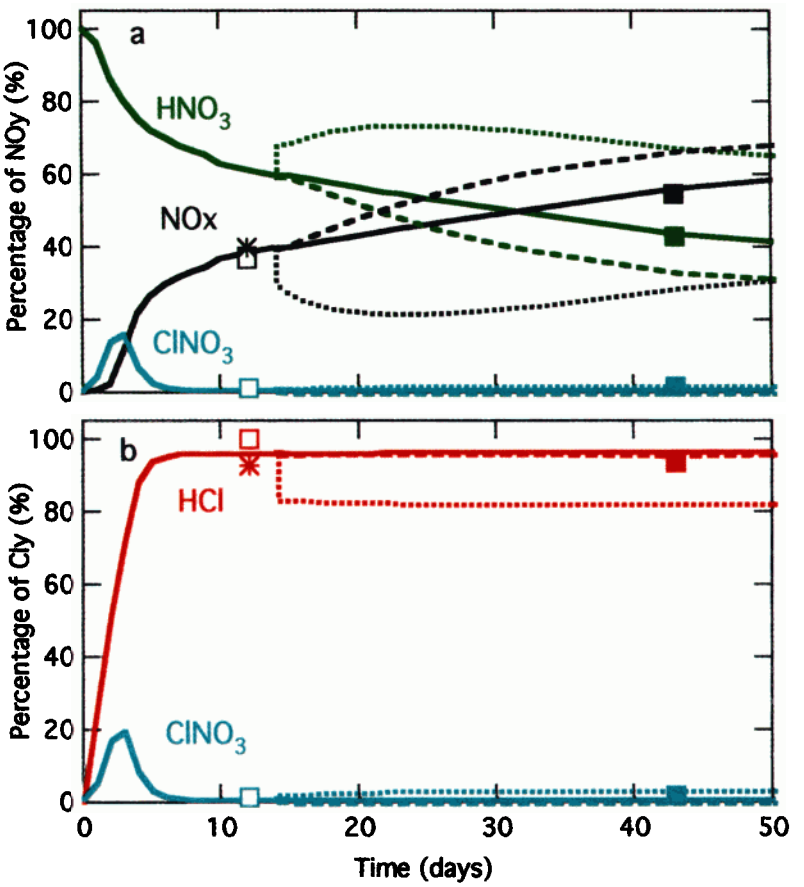

Plate 6. The time evolution of modeled abundances of (a) HNO_3, NO_x, and $ClNO_3$ shown as a percentage of available NO_y and (b) HCl and $ClNO_3$ shown as a percentage of available Cl_y. The model was run for a level of 409 K and was initialized assuming a warming (to above 200 K) following a hypothetical PSC event (on day 0) in which all Cl_y was activated, and HNO_3 accounted for all NO_y (solid lines, color-coded by species, as indicated). Initialization abundances of O_3 (0.128 ppm), CH_4 (1.10 ppm), H_2O (2.87 ppm), Cl_y (2.38 ppb), and NO_y (2.92 ppb) were input into the model as measured (or inferred from measured values) inside the vortex at 409 K, and the model was run assuming constant solar conditions for a latitude of 69°S on October 11 with an albedo of 0.8. On day 14, extravortex air was simulated to mix into the vortex core with measured (or inferred) abundances of O_3 (0.98 ppm), CH_4 (1.46 ppm), H_2O (4.3 ppm), HCl (0.768 ppb), $ClNO_3$ (0.062 ppb), NO_x (0.597 ppb), and HNO_3 (2.23 ppb), such that the resulting air mass was composed of 50% extravortex air and 50% vortex air (dotted lines). The symbols (open squares for ER-2, solid squares for ATMOS, and asterisks for HALOE) represent species distributions measured inside the vortex at 409 K, color coded by species as indicated by the labels. The dashed lines show a calculation in which temperatures were lowered to 193 K, and particle surface area was increased from 2 to 9 $\mu m^2/cm^3$ with a mean radius of 0.4 μm, to simulate the response to a PSC-type event.

NO_x. Growth of HCl to >90% of Cl_y occurs more rapidly if NO_y has not been significantly depleted. Although an increase in NO_y may be expected to increase the production rate of $ClNO_3$ via (R1), under ozone-depleted conditions, NO_x is preferentially partitioned into NO. The rate of (R4) and hence production of HCl via (R2) is instead enhanced when NO_y is increased.

On day 14 (October 13), as the species distributions approached values measured in the vortex (color-coded symbols), we allowed extravortex air to mix into the vortex core with measured species abundances of 0.98 ppm O_3, 1.46 ppm CH_4, 4.3 ppm H_2O, 0.77 ppb HCl, 0.062 ppb $ClNO_3$, 0.597 ppb NO_x, and 2.23 ppb HNO_3, such that the resulting air mass was made up of 50% extravortex air and 50% vortex air (dotted lines). The solar conditions for these calculations (starting on day 14) evolved with time in order to provide a better simulation of the time period between the October and November measurements. The results show that if a significant amount of extravortex air had mixed into the vortex, the new steady state partitioning of Cl_y and NO_y would have been established quickly and would have been dramatically different from the case in which no extravortex air mixed into the vortex (solid lines). This latter case, designed to simulate a completely isolated vortex, is in much better agreement with the November observations (solid squares). For the test case shown in Plate 6, the NO_y partitioning in the vortex is particularly sensitive to the influx of extravortex air. These changes are predominantly attributable to the increase in vortex $[O_3]$ (from 0.128 to 0.554 ppm) as edge air was mixed with vortex air in the model.

This analysis is more sensitive than an analysis based solely on changes in tracer abundances in the vortex during this time period. As discussed above, identifying mixing into the vortex using tracer correlations is complicated by perturbations to the tracer relationships caused by denitrification and ozone loss. Ascent or descent of air in the vortex can lead to uncertainties in conclusions drawn from tracer profiles, and experimental uncertainties are too large (particularly for the remote measurements in the lower stratosphere) to identify even the sign of a change in vortex $[O_3]$ between the October and November measurements (see Figure 1).

Plate 7 shows the calculated variation of the ratio $[NO_x]$:$[HNO_3]$ with the percentage of extravortex air mixed into the vortex compared with observations made by ATMOS in November. We initialized these calculations based on the measurements made in October at each potential temperature. The mean value of the $[NO_x]$:$[HNO_3]$ ratio from measurements

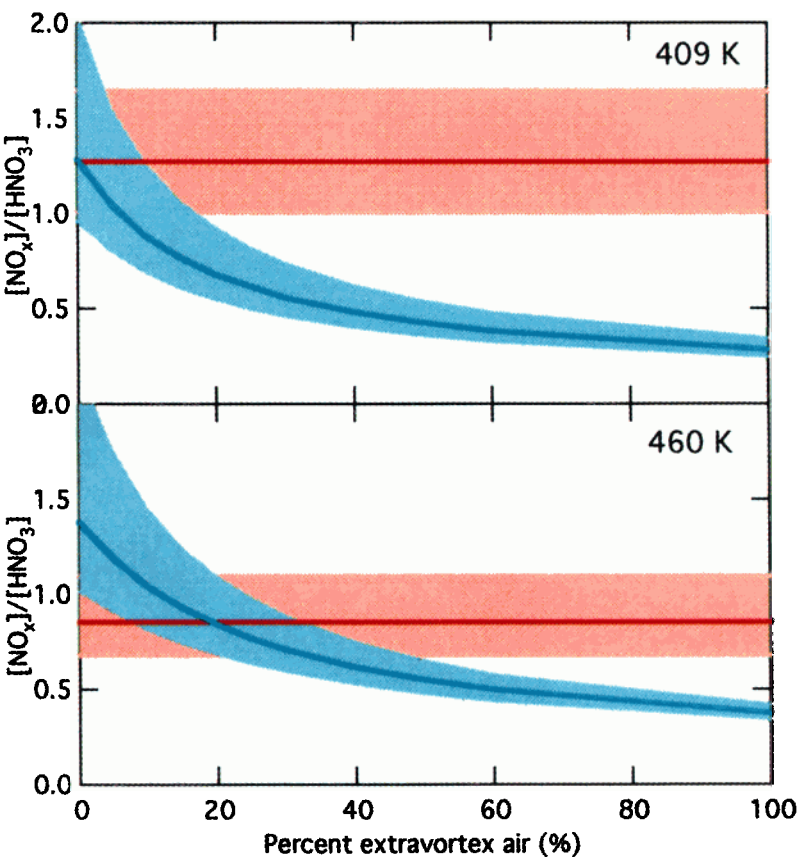

Plate 7. The ratio $[NO_x]$:$[HNO_3]$, calculated as a function of the percentage of extravortex air mixed into the vortex, compared with observations made by ATMOS in November. We initialized these calculations based on the measurements made in October at (top) 409 K and (botom) 460 K. The pink shaded regions indicate experimental uncertainties in the $[NO_x]$:$[HNO_3]$ ratio (including both systematic and random error), and the blue shaded regions demonstrate the uncertainties in the calculated values that result from experimental uncertainties in measurements of $[O_3]$. We based the calculations at 409 K on the in situ measurements of $[O_3]$, which have better accuracy and precision in the lower stratosphere than the remote observations.

made in November is most consistent with no mixing of extravortex air into the vortex core at 409 K and ~20% of extravortex air mixed into the vortex at 460 K during October and early November. The pink shaded regions indicate experimental uncertainties in the $[NO_x]$:$[HNO_3]$ ratio (including both systematic and random error), and the blue shaded regions demonstrate the uncertainties in the calculated values that result from experimental uncertainties in measurements of $[O_3]$. We based the calculations at 409 K on the in situ measurements of $[O_3]$, which are more accurate in the lower stratosphere than the remote observations. Given these estimates of the experimental error, the data can support a final composition in mid-November in the vortex core of 17% recent extravortex air at 409 K and as much as 48% at 460 K. The [HCl]:$[ClNO_3]$ ratio can similarly be used to quantify the amount of extravortex air mixed into the vortex, and the conclusions derived from the $[NO_x]$:$[HNO_3]$ ratio are consistent with those provided by [HCl]:$[ClNO_3]$. Values of $[ClNO_3]$ were extremely small and difficult to measure inside the vortex, however, leading to large experimental uncertainties for [HCl]:$[ClNO_3]$ and a less conclusive result than provided by the $[NO_x]$:$[HNO_3]$ ratio. These conclusions are in good agreement with a more rigorous analysis of the polar vortex dynamics during this time period [*Manney et al.*, 1999].

5.6. The Effects of Heterogeneous Chemistry on Cl_y and NO_y Partitioning

Temperatures within the Antarctic vortex were persistently below 195 K through early November 1994 [*Manney et al.*, 1996]. At these temperatures, conversion of Cl_y reservoir species to reactive radicals usually proceeds rapidly via the following heterogeneous mechanisms [e.g., *Solomon et al.*, 1986; *McElroy et al.*, 1986; *Molina et al.*, 1987; *Tolbert et al.*, 1987]:

(R13) $$HCl + ClNO_3 \rightarrow Cl_2 + HNO_3,$$

(R14) $$ClNO_3 + H_2O \rightarrow HOCl + HNO_3,$$

(R15) $$HCl + HOCl \rightarrow Cl_2 + H_2O.$$

These reactions have been implicated in the conversion of HCl and $ClNO_3$ to Cl and ClO that was observed to occur in the vortex between June and September 1994 [*Tuck et al.*, 1995b; *Grooss et al.*, 1997; *Jaeglé et al.*, 1997; *Kawa et al.*, 1997]. Since HNO_3 is a by-product of (R13) and (R14), an increase in the rates of these reactions should additionally lead to a significant change in the partitioning of NO_y.

A time-dependent calculation similar to the one described above was performed to identify potential perturbations to the Cl_y and NO_y partitioning initiated by heterogeneous chemistry occurring on or in PSC particles in the springtime Antarctic vortex. Cl_y and NO_y species were allowed to evolve following a hypothetical PSC event in which Cl_y was fully activated (Plate 6). On day 14 (October 13), after the abundances of these species approached values measured in the vortex, a PSC-type event was simulated. The temperature was lowered to 193 K, and the surface area was increased from 2 to 9 $\mu m^2/cm^3$ with a mean radius of 0.4 μm, consistent with observations of PSCs during July [*Del Negro et al.*, 1997; *Kawa et al.*, 1997]. Although low temperatures and high surface areas were maintained for weeks in the model, heterogeneous processes had little effect on calculated Cl_y and NO_y partitioning, as shown by the dashed lines in Plate 6. Low values of $[ClNO_3]$ in the vortex diminished the effectiveness of (R13) and (R14). The rate of (R15) was limited by the availability of HOCl, which is generally produced by the gas-phase reaction

(R16) $$ClO + HO_2 \rightarrow HOCl + O_2.$$

Under low-ozone conditions, however, ClO abundances are reduced, leading to a reduction in the rate of (R16). Changes in the NO_y partitioning are attributable to an increase in the rate of (R9a) with decreasing temperature [*Brown et al.*, 1999a].

With the small amounts of $[O_3]$ observed inside the vortex, dropping the temperature to 190 K and increasing the surface area to 10 $\mu m^2/cm^3$ did not force the heterogeneous chemistry to proceed fast enough to perturb the Cl_y and NO_y partitioning. The model thus predicts that once ozone is depleted and Cl_y is partitioned predominantly into HCl, heterogeneous reactions will have little effect on Cl_y and NO_y partitioning. This result is confirmed by the apparent lack of change in $[HCl]/[Cl_y]$ and $[NO_x]/[NO_y]$ throughout October and early November, despite temperatures low enough to initiate heterogeneous processes.

An influx of ozone-rich air into the vortex, however, would have made the vortex much more susceptible to low-temperature heterogeneous chemistry. With an increase in $[O_3]$ that would have accompanied an influx of 50% extravortex air at 409 K, model calculations indicate that the reservoir species HCl and $ClNO_3$ would have been nearly fully activated within a few days at 193 K. These results support the conclusion that little extravortex air had mixed into the lower part of the vortex during October and early November.

5.7. Evolution of Cl_y and NO_y Partitioning in the Springtime Polar Vortices

Plate 8 summarizes the evolutionary phases of species in the Cl_y (left panels) and NO_y (right panels) families throughout the polar winter and spring and demonstrates the differences in Cl_y and NO_y recovery in the spring depending on whether the vortex is only moderately (top panels) or, in contrast, is severely (bottom panels) depleted in ozone during the late winter/early spring. The former case (top panels) is currently more characteristic of the Arctic vortex during years when Cl_y is significantly activated, whereas the latter (bottom panels) is more representative of the Antarctic vortex.

During the fall, nearly all Cl_y is either HCl or $ClNO_3$. Under moderate to low aerosol conditions, HCl is the larger reservoir for Cl_y [e.g., *Dessler et al.*, 1995; *Michelsen et al.*, 1996; *Webster et al.*, 1998]. When temperatures drop below ~195 K, heterogeneous reactions (R13), (R14), and (R15) rapidly convert HCl and $ClNO_3$ to Cl_2. If sunlight is available, or when it becomes available, Cl_2 is photolyzed, producing reactive chlorine radicals that participate in the catalytic destruction of ozone. As temperatures increase in the spring (or ozone loss is complete), heterogeneous activation ceases, and active chlorine is reconverted to HCl and $ClNO_3$. If O_3 has been severely depleted (bottom left panel of Plate 8), a steady state condition is quickly reached in which HCl makes up most of the Cl_y. This state is maintained until extravortex air is mixed into the vortex or the vortex breaks up. If, on the other hand, O_3 is only moderately depleted (top left panel of Plate 8), active chlorine is preferentially reconverted to $ClNO_3$ in the spring. Regaining the steady state condition for moderate ozone abundances under these circumstances is slow and can take a couple of months, by which time the vortex has usually broken up. Thus the Antarctic vortex can spend most of the

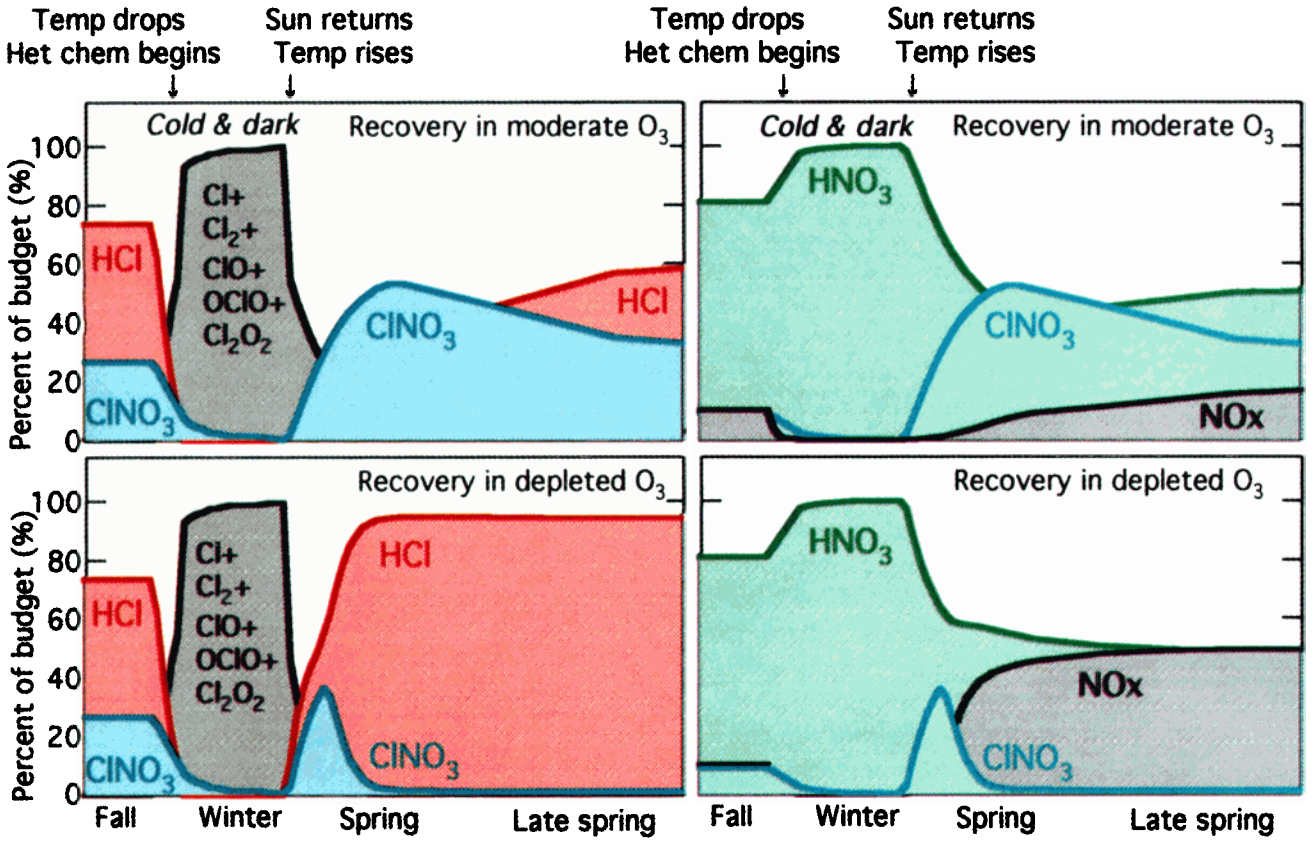

Plate 8. Schematic summary of the evolution of Cl_y (left panels) and NO_y (right panels) species abundances through the life cycle of the polar vortex. Species abundances are represented as a percentage of available Cl_y (left panels) or NO_y (right panels). The differences in springtime recovery are compared for a situation in which ozone has been only moderately depleted (top panels) or severely depleted (bottom panels). The conditions demonstrated in the top panels are currently more characteristic of the Arctic vortex, whereas the recovery shown in the bottom panels is more representative of the Antarctic vortex.

spring in photochemical steady state, whereas the Arctic vortex is generally not in steady state once it cools in early winter. Such contrasts between the springtime Arctic and Antarctic vortices are particularly extreme, given the longer lifetime of the Antarctic vortex.

The right two panels of Plate 8 summarize the corresponding evolution of NO_y species through the life cycle of the polar vortex. HNO_3 is the most significant component of the NO_y family in the lower stratosphere. As the vortex cools in the early winter, and heterogeneous processes are accelerated, HNO_3 accommodates nearly all of NO_y. In late winter/early spring when the vortex warms or ozone destruction is complete, production of HNO_3 via heterogeneous mechanisms is greatly diminished. If O_3 is severely depleted (bottom right panel of Plate 8), the rate of (R8) and thus the production rate of HNO_3 is reduced, and the abundance of HNO_3 quickly decreases to a steady state value of ~50% of NO_y. The rest of NO_y is in the form of NO_x. If O_3 is only moderately depleted (top right panel of Plate 8), the balance in the NO_y budget is controlled by the rapid production of $ClNO_3$, which depletes NO_x. The rate at which the NO_y-species distribution reaches steady state values is determined by how quickly HCl and $ClNO_3$ reach steady state conditions, which may not occur prior to the breakup of the vortex when O_3 is not fully depleted.

6. Conclusions

Based on an analysis of measured abundances of long-lived tracers and shorter-lived photochemically active species, we have been able to investigate the interplay between transport and chemistry in and around the springtime Antarctic vortex. Correlations of $[CH_4]$ relative to $[N_2O]$ demonstrate that although some mixing of extravortex air into the polar vortex had occurred by November 1994, the amount of such mixing during middle to late spring appears to be much less than has been inferred from similar studies of Arctic correlations [*Michelsen et al.*, 1998a,b; *Kondo et al.*, 1999; R. A. Plumb et al., submitted paper, 1999; *Rex et al.*, 1999]. This conclusion is consistent with previous studies that have shown that the Antarctic vortex is more isolated than its Arctic counterpart [*Manney et al.*, 1994, 1999; *Plumb et al.*, 1994; *Dahlberg and Bowman*, 1995; *Tuck et al.*, 1995a]. During October 1994, the vortex core appears to have been very well isolated near 410 K, as indicated by the persistence of steady state conditions characterized by $[HCl]/[Cl_y]>0.9$ and $[NO_x]/[NO_y]>0.4$. An influx of extravortex air into the vortex would have lead to lower $[HCl]/[Cl_y]$ and $[NO_x]/[NO_y]$ and forced the vortex Cl_y partitioning away from steady state. Near 460 K, the partitioning of NO_y species suggests that some extravortex air (~20%) may have mixed into the vortex during the spring.

This result is consistent with a recent analysis of the vortex dynamics during October-November 1994 [*Manney et al.*, 1999]. In addition, during October and early November, vortex temperatures were persistently below 195 K, low enough to initiate heterogeneous processes known to activate Cl_y and repartition NO_y to HNO_3 during winter [*Manney et al.*, 1996]. Under low-ozone conditions, these processes are ineffective at perturbing the partitioning of Cl_y and NO_y. Had ozone-rich extravortex air mixed into the vortex during this time period, the vortex Cl_y and NO_y partitioning would have been more susceptible to the low-temperature events, lending further support to the conclusion that the influx of extravortex air was small during spring 1994.

In the vortex-edge region, isentropic mixing appears to have been slow enough, relative to the influx of vortex and extravortex air into this region, to allow correlations of $[O_3]$:$[N_2O]$, $[NO_y]$:$[N_2O]$, and $[CH_4]$:$[N_2O]$ to span the wide range of values defined by vortex and extravortex air. Some mixing does appear to occur in this region, however, leading to large scatter in the vertical profiles and deviations in the $[CH_4]$:$[N_2O]$ correlation that are representative of descent (of upper stratospheric and mesospheric air) followed by mixing (with air from lower altitudes). A portion of this descent appears to have occurred in the edge, as shown by an analysis of the springtime vortex dynamics [*Manney et al.*, 1999]. Mixing of air from the inner vortex into the edge is also indicated by values of inferred $[ClNO_3]$ from observations made in October that are up to 4 times higher than steady state model predictions and observations made a month later. These observations suggest that vortex air with high levels of active chlorine had mixed into the edge, where $[O_3]$ was relatively high, leading to recovery of active chlorine in the edge into $ClNO_3$ instead of HCl. By November, the Cl_y partitioning was more consistent with steady state values.

These results demonstrate that, when ozone has been severely depleted in the vortex, recovery of PSC-perturbed species distributions to steady state conditions occurs rapidly (within a couple of weeks) to a state in which HCl comprises nearly all of Cl_y, and NO_x makes up almost half of NO_y. This state is maintained until extravortex air is entrained into the vortex or the vortex breaks up. If ozone is only moderately depleted, recovery of the Cl_y and NO_y partitioning takes place via an intermediate phase in which $ClNO_3$ comprises a large fraction of Cl_y and NO_y. Recovery under these conditions occurs over several months and may not be complete before the vortex breaks up.

Acknowledgments. We thank team members of the ASHOE/MAESA mission and the ATMOS, HALOE, and SAGE II science teams, with special thanks to L. Jaeglé for helpful comments and preliminary calculations, D. W. Fahey, R. S. Gao, L. A. Del Negro, R. C. Wamsley, and E. R. Keim for providing in situ NO, NO_2, and NO_y measurements, M. H. Proffitt and K. Aikin for in situ O_3 measurements, R. M. Stimpfle, D. W. Kohn, and J. G. Anderson for in situ ClO measurements, P. A. Newman for PV associated with the ER-2 data, and A. F Tuck and W. H. Brune for the roles they played as project scientists in the planning and implementation of the ER-2 mission. Part of the research described in this paper was carried out at the Jet Propulsion Laboratory, California Institute of Technology, under contract with the National Aeronautics and Space Administration (NASA). This work was also supported by the NASA Atmospheric Chemistry Modeling and Analysis Program and SAGE III science team.

References

Abbatt, J. P D , Interactions of HBr, HCl, and HOBr with supercooled sulfuric acid solutions of stratospheric composition, *J. Geophys. Res.*, *100*, 14,009-14,017, 1995.

Abrams, M. C., et al., On the assessment and uncertainty of atmospheric trace gas burden measurements with high-resolution infrared solar occultation spectra from space by the ATMOS experiment, *Geophys. Res. Lett.*, *23*, 2337-2340, 1996a.

Abrams, M. C., et al., ATMOS/ATLAS-3 observations of long-lived tracers and descent in the Antarctic vortex in November 1994, *Geophys. Res. Lett.*, *23*, 2345-2348, 1996b.

Anderson, J. G., W. H. Brune, and M. H. Proffitt, Ozone destruction by chlorine radicals within the Antarctic vortex: The spatial and temporal evolution of ClO-O_3 anticorrelation based on in situ ER-2 data, *J. Geophys. Res.*, *94*, 11,465-11,479, 1989.

Battin-Leclerc, F., I. K. Kim, R. K. Talukdar, R. W. Portmann, A. R. Ravishankara, R. Steckler, and D. Brown, Rate coefficients for the reactions of OH and OD with HCl and DCl between 200 and 400 K, *J. Phys. Chem. A*, *103*, 3237-3244, 1999.

Becker, G., R. Müller, D. S. McKenna, M. Rex, and K. Carslaw, Ozone loss rates in the Arctic stratosphere in the winter 1991/92: Model calculations compared with Match results, *Geophys. Res. Lett.*, *25*, 4325-4328, 1998.

Bird, J. C., S. R. Pal, A. I. Carswell, D. P. Donovan, G. L. Manney, J. M. Harris, and O. Uchino, Observations of ozone structures in the Arctic polar vortex, *J. Geophys. Res.*, *102*, 10,785-10,800, 1997.

Blom, C. E., H. Fischer, N. Glatthor, T. Gulde, M. Höpfner, and C. Piesch, Spatial and temporal variability of $ClONO_2$, HNO_3, and O_3 in the Arctic winter of 1992/1993 as obtained by airborne infrared emission spectroscopy, *J. Geophys. Res.*, *100*, 9109-9114, 1995.

Bowman, K. P., Large-scale isentropic mixing properties of the Antarctic polar vortex from analyzed winds, *J. Geophys. Res.*, *98*, 23,013-23,027, 1993.

Brown, S. S., R. K. Talukdar, and A. R. Ravishankara, Reconsideration of the rate constant for the reaction of hydroxyl radicals with nitric acid, *J. Phys. Chem. A*, *103*, 3031-3037, 1999a.

Brown, S. S , R. K. Talukdar, and A. R. Ravishankara, Rate constant for the reaction $OH+NO_2+M \rightarrow HNO_3+M$ under stratospheric conditions, *Chem. Phys. Lett.*, *299*, 277-284, 1999b.

Brühl, C., et al., Halogen Occultation Experiment ozone channel validation, *J. Geophys. Res.*, *101*, 10,217-10,240, 1996.

Chang, A. Y., et al., A comparison of measurements from ATMOS and instruments aboard the ER-2 aircraft: Tracers of atmospheric transport, *Geophys. Res. Lett.*, *23*, 2389-2392, 1996a.

Chang, A. Y., et al., A comparison of measurements from ATMOS and instruments aboard the ER-2 aircraft: Halogenated gases, *Geophys. Res. Lett.*, *23*, 2393-2396, 1996b.

Chen, P., The permeability of the Antarctic vortex edge, *J. Geophys. Res.*, *99*, 20,563-20,571, 1994.

Chipperfield, M. P., J. A. Pyle, C. E. Blom, N. Glatthor, M. Höpfner, T. Gulde, C. Piesch, and P. Simon, The variability of $ClONO_2$ and HNO_3 in the Arctic polar vortex: Comparison of Transall Michelson interferometer for passive atmospheric sounding measurements and three-dimensional model results, *J. Geophys. Res.*, *100*, 9115-9129, 1995.

Chipperfield, M. P., E. R. Lutman, J. A. Kettleborough, J. A. Pyle, and A. E. Roche, Model studies of chlorine activation and formation of a $ClONO_2$ collar in the Arctic polar vortex, *J. Geophys. Res.*, *102*, 1467-1478, 1997.

Dahlberg, S. P., and K. P Bowman, Isentropic mixing in the Arctic stratosphere during the 1992-1993 and 1993-1994 winters, *Geophys. Res. Lett.*, *22*, 1237-1240, 1995.

Del Negro, L. A., et al., Evaluating the role of NAT, NAD, and liquid $H_2SO_4/H_2O/HNO_3$ solutions in Antarctic polar stratospheric cloud aerosol: Observations and implications, *J. Geophys. Res.*, *102*, 13,255-13,282, 1997.

DeMore, W B., S. P. Sander, C. J. Howard, A. R. Ravishankara, D. M. Golden, C. E. Kolb, R. F. Hampson, M. J. Kurylo, and M. J. Molina, Chemical kinetics and photochemical data for use in stratospheric modeling, Evaluation number 12, *JPL Publ. 97-4*, 1997.

Dessler, A. E., et al., Correlated observations of HCl and $ClONO_2$ from UARS and implications for stratospheric chlorine partitioning, *Geophys Res. Lett.*, *22*, 1721-1724, 1995.

deZafra, R. L., M. Jaramillo, A. Parrish, P. M. Solomon, B. Connor, and J. Barnett, High concentrations of chlorine monoxide at low altitudes in the Antarctic spring stratosphere: Diurnal variation, *Nature*, *328*, 408-411, 1987.

deZafra, R. L., M. Jaramillo, J. Barnett, L. K. Emmons, P. M. Solomon, and A. Parrish, New observations of a large concentration of ClO in the springtime lower stratosphere over Antarctica and its implications for ozone-depleting chemistry, *J. Geophys. Res.*, *94*, 11,423-11,428, 1989.

Donaldson, D. J., A. R. Ravishankara, and D. R. Hanson, Detailed study of HOCl+HCl→Cl_2+H_2O in sulfuric acid, *J. Phys. Chem. A*, *101*, 4717-4725, 1997.

Douglass, A. R., M. R. Schoeberl, R. S. Stolarski, J. W. Waters, J. M. Russell III, A. E. Roche, and S. T. Massie, Interhemispheric differences in springtime production of HCl and $ClONO_2$ in the polar vortices, *J. Geophys. Res.*, *100*, 13,967-13,978, 1995.

Dunkerton, T. J., and D. P. Delisi, Evolution of potential vorticity in the winter stratosphere of January-February, 1979, *J. Geophys. Res.*, *91*, 1199-1208, 1986.

Eluszkiewicz, J., R. A. Plumb, and N. Nakamura, Dynamics of wintertime stratospheric transport in the Geophysical Fluid Dynamics Laboratory SKYHI general circulation model, *J. Geophys. Res.*, *100*, 20,883-20,900, 1995.

Fahey, D. W., et al., In situ measurements constraining the role of sulfate aerosols in mid-latitude ozone depletion, *Nature*, *363*, 509-514, 1993.

Farmer, C. B., G. C. Toon, P. W. Shaper, J.-F. Blavier, and L. L. Lowes, Stratospheric trace gases in the spring 1986 Antarctic atmosphere, *Nature*, *329*, 126-130, 1987.

Gao, R. S., E. R. Keim, E. L. Woodbridge, S. J. Ciciora, M. H. Proffitt, T. L. Thompson, R. J. McLaughlin, and D. W. Fahey, New photolysis system for NO_2 measurements in the lower stratosphere, *J. Geophys. Res.*, *99*, 20,673-20,681, 1994.

Gao, R. S., et al., A comparison of observations and model simulations of NO_x/NO_y in the lower stratosphere, *Geophys. Res. Lett.*, *26*, 1153-1156, 1999.

Geller, M. A., V. Yudin, A. R. Douglass, J. W. Waters, L. S. Elson, A. E. Roche, and J. M. Russell III, UARS PSC, $ClONO_2$, HCl, and ClO measurements in early winter: Additional verification of the paradigm for chlorine activation, *Geophys. Res. Lett.*, *22*, 2937-2940, 1995.

Gierczak, T., J. B. Burkholder, and A. R. Ravishankara, Temperature dependent rate coefficient for the reaction: $O(^3P)+NO_2 \rightarrow NO+O_2$, *J. Phys. Chem. A*, *103*, 877-883, 1999.

Gordley, L. L., et al., Validation of nitric oxide and nitrogen dioxide measurements made by the Halogen Occultation Experiment for UARS platform, *J. Geophys. Res.*, *101*, 10,241-10,266, 1996.

Grooss, J.-U., R. B. Pierce, P. J. Crutzen, W. L. Grose, and J. M. Russell III, Re-formation of chlorine reservoirs in southern hemisphere polar spring, *J. Geophys. Res.*, *102*, 13,141-13,152, 1997.

Grose, W. L., G. S. Lingenfelser, J. M. Russell III, R. B. Pierce, T. D. Fairlie, and M. H. Proffitt, Intercomparison of ozone measurements in the lower stratosphere from the UARS Halogen Occultation Experiment and the ER-2 UV absorption photometer, *J. Geophys. Res.*, *102*, 13,135-13,140, 1997.

Gunson, M. R., et al., The atmospheric trace molecule spectroscopy (ATMOS) experiment: Deployment on the ATLAS space shuttle missions, *Geophys. Res. Lett.*, *23*, 2333-2336, 1996.

Hanson, D. R., Reaction of $ClONO_2$ with H_2O and HCl in sulfuric acid and $HNO_3/H_2SO_4/H_2O$ mixtures, *J. Phys. Chem. A*, *102*, 4794-4807, 1998.

Hartmann, D. L., L. E. Heidt, M. Loewenstein, J. R. Podolske, J. Vedder, W. L. Starr, and S. E. Strahan, Transport into the south polar vortex in early spring, *J. Geophys. Res.*, *94*, 16,779-16,796, 1989.

Herman, R. L., et al., Tropical entrainment time scales inferred from stratospheric N_2O and CH_4 observations, *Geophys. Res. Lett.*, *25*, 2781-2784, 1998.

Jaeglé, L., et al., Evolution and stoichiometry of heterogeneous processing in the Antarctic stratosphere, *J. Geophys. Res.*, *102*, 13,235-13,253, 1997.

Kawa, S. R., et al., Photochemical partitioning of the reactive nitrogen and chlorine reservoirs in the high latitude stratosphere, *J. Geophys. Res.*, *97*, 7905-7923, 1992.

Kawa, S. R., et al., Activation of chlorine in sulfate aerosol as inferred from aircraft observations, *J. Geophys. Res.*, *102*, 3921-3933, 1997.

Kondo, Y., U. Schmidt, T. Sugita, A. Engel, M. Koike, P. Aimedieu, M. R. Gunson, and J. Rodriguez, NO_y correlation with N_2O and CH_4 in the midlatitude stratosphere, *Geophys. Res. Lett.*, *23*, 2369-2372, 1996.

Kondo, Y., et al., NO_y-N_2O correlation observed inside the Arctic vortex in February 1997: Dynamical and chemical effects, *J. Geophys. Res.*, *104*, 8215-8224, 1999.

Lipson, J. B., M. J. Elrod, T. W. Beiderhase, L. T. Molina, and M. J. Molina, Temperature dependence of the rate constant and branching ratio for the OH+ClO reaction, *J. Chem. Soc., Faraday Trans.*, *93*, 2665-2673, 1997.

Manney, G. L., and R. W. Zurek, Interhemispheric comparison of the development of the stratospheric polar vortex during fall: A 3-dimensional perspective for 1991-1992, *Geophys. Res. Lett.*, *20*, 1275-1278, 1993.

Manney, G. L., R. W. Zurek, A. O'Neill, and R. Swinbank, On the motion of air through the stratospheric polar vortex, *J. Atmos. Sci.*, *51*, 2973-2994, 1994.

Manney, G. L., R. Swinbank, and A. O'Neill, Stratospheric meteorological conditions for the 3-12 Nov 1994 ATMOS/ATLAS-3 measurements, *Geophys. Res. Lett.*, *23*, 2409-2412, 1996.

Manney, G. L., J. C. Bird, D. P. Donovan, T. J. Duck, J. A. Whiteway, S. R. Pal, and A. I. Carswell, Modeling ozone laminae in ground-based Arctic wintertime observations using trajectory calculations and satellite data, *J. Geophys. Res.*, *103*, 5797-5814, 1998.

Manney, G. L., H. A Michelsen, M. L. Santee, M. R. Gunson, A. E. Roche, and N. J. Livesey, Polar vortex dynamics during spring and fall diagnosed using trace gas observations from the Atmospheric Trace Molecule Spectroscopy instrument, *J. Geophys. Res.*, *104*, 18,841-18,866, 1999.

McElroy, M. B., R. J. Salawitch, S. C. Wofsy, and J. A. Logan, Reductions of Antarctic ozone due to synergistic interactions of chlorine and bromine, *Nature*, *321*, 759-762, 1986.

McIntyre, M. E., The stratospheric polar vortex and sub-vortex: Fluid dynamics and midlatitude ozone loss, *Philos. Trans. R. Soc. London, Ser. A*, *352*, 227-240, 1995.

Michelsen, H. A., et al., Stratospheric chlorine partitioning: Constraints from shuttle-borne measurements of [HCl], [$ClNO_3$], and [ClO], *Geophys. Res. Lett.*, *23*, 2361-2364, 1996.

Michelsen, H. A., G. L. Manney, M. R. Gunson, and R. Zander, Correlations of stratospheric abundances of NO_y, O_3, N_2O, and CH_4 derived from ATMOS measurements, *J. Geophys. Res.*, *103*, 28,347-28,359, 1998a.

Michelsen, H. A., G. L. Manney, M. R. Gunson, C. P. Rinsland, and R. Zander, Correlations of stratospheric abundances of CH_4 and N_2O derived from ATMOS measurements, *Geophys. Res. Lett.*, *25*, 2777-2780, 1998b.

Michelsen, H. A., et al., Intercomparison of ATMOS, SAGE II, and ER-2 observations in Arctic vortex and extra-vortex air masses during spring 1993, *Geophys. Res. Lett.*, *26*, 291-294, 1999a.

Michelsen, H. A., C. M. Spivakovsky, and S. C. Wofsy, Aerosol-mediated partitioning of stratospheric Cl_y and NO_y at temperatures above 200 K, *Geophys. Res. Lett.*, *26*, 299-302, 1999b.

Mickley, A. R., J. P. D. Abbatt, J. E. Frederick, and J. M. Russell III, Evolution of chlorine and nitrogen species in the lower stratosphere during Antarctic spring: Use of tracers to determine chemical change, *J. Geophys. Res.*, *102*, 21,479-21,491, 1997.

Molina, L. T., and M. J. Molina, Production of Cl_2O_2 from the self-reaction of the ClO radical, *J. Phys. Chem*, *91*, 433-436, 1987.

Molina, M. J., T.-L. Tso, L. T. Molina, and F. C.-Y. Wang, Antarctic stratospheric chemistry of chlorine nitrate, hydrogen chloride, and ice: Release of active chlorine, *Science*, *238*, 1253-1257, 1987.

Müller, R., Th. Peter, P. J. Crutzen, H. Oelhaf, G. P. Adrian, T. v. Clarmann, A. Wegner, U. Schmidt, and D. Lary, Chlorine chemistry and the potential for ozone depletion in the arctic stratosphere in the winter of 1991/92, *Geophys. Res. Lett.*, *21*, 1427-1430, 1994.

Nash, E. R., P. A. Newman, J. R. Rosenfield, and M. R. Schoeberl, An objective determination of the polar vortex using Ertel's potential vorticity, *J. Geophys. Res.*, *101*, 9471-9478, 1996.

Osterman, G. B., B. Sen, G. C. Toon, R. J. Salawitch, J. J. Margitan, J.-F. Blavier, D. W. Fahey, and R. S. Gao, Partitioning of NO_y species in the summer Arctic stratosphere, *Geophys. Res. Lett.*, *26*, 1157-1160, 1999.

Park, J. H., et al., Validation of Halogen Occultation Experiment CH_4 measurements from UARS, *J. Geophys. Res.*, *101*, 10,183-10,203, 1996.

Pierce, R. B., J.-U. Grooss, W. L. Grose, J. M. Russell III, P. J. Crutzen, T. D. Fairlie, and G. Lingenfelser, Photochemical calculations along air mass trajectories during ASHOE/MAESA, *J. Geophys. Res.*, *102*, 13,153-13,167, 1997.

Plumb, R. A., and M. K. W. Ko, Interrelationships between mixing ratios of long-lived stratospheric constituents, *J. Geophys. Res.*, *97*, 10,145-10,156, 1992.

Plumb, R. A., D. W. Waugh, R. J. Atkinson, P. A. Newman, L. R. Lait, M. R. Schoeberl, E. V. Browell, A. J. Simmons, and M. Loewenstein, Intrusions into the lower stratospheric Arctic vortex during the winter of 1991-1992, *J. Geophys. Res.*, *99*, 1089-1105, 1994.

Prather, M. J., and A. H. Jaffe, Global impact of the Antarctic ozone hole: Chemical propagation, *J. Geophys. Res.*, *95*, 3473-3492, 1990.

Proffitt, M. H., and R. J. McLaughlin, Fast response dual beam UV absorption ozone photometer suitable for use on stratospheric balloons, *Rev. Sci. Instrum.*, *54*, 1719-1728, 1983.

Rex, M., et al., Prolonged stratospheric ozone loss in the 1995-96 Arctic winter, *Nature*, *389*, 835-838, 1997.

Rex, M., et al., Subsidence, mixing, and denitrification of Arctic polar vortex air measured during POLARIS, *J. Geophys. Res.*, in press, 1999.

Rinsland, C. P., et al., ATMOS/ATLAS-3 measurements of stratospheric chlorine and reactive nitrogen partitioning inside and outside the November 1994 Antarctic vortex, *Geophys. Res. Lett.*, *23*, 2365-2368, 1996.

Rinsland, C. P., et al., Polar stratospheric descent of NO_y and CO and Arctic denitrification during winter 1992-93, *J. Geophys. Res.*, *104*, 1847-1861, 1999.

Roche, A. E., et al., Observations of lower-stratospheric $ClONO_2$, HNO_3, and aerosol by the UARS CLAES experiment between January 1992 and April 1993, *J. Atmos. Sci.*, *51*, 2877-2902, 1994.

Russell, J. M., III, et al., Validation of hydrogen chloride measurements made by the Halogen Occultation Experiment from the UARS platform, *J. Geophys. Res.*, *101*, 10,151-10,162, 1996.

Salawitch, R. J., et al., Loss of ozone in the Arctic vortex for the winter of 1989, *Geophys. Res. Lett.*, *17*, 561-564, 1990.

Santee, M. L., et al., Chlorine deactivation in the lower stratospheric polar regions during late winter: Results from UARS, *J. Geophys. Res.*, *101*, 18,835-18,859, 1996.

Santee, M. L., G. L. Manney, L. Froidevaux, W. G. Read, and J. W. Waters, Six years of UARS Microwave Limb Sounder HNO_3 observations: Seasonal, interhemispheric, and interannual variations in the lower stratosphere, *J. Geophys. Res.*, *104*, 8225-8246, 1999.

Schoeberl, M. R., L. R. Lait, P. A. Newman, and J. E. Rosenfield, The structure of the polar vortex, *J. Geophys. Res.*, *97*, 7859-7882, 1992.

Schoeberl, M. R., A. R. Douglass, S. R. Kawa, A. E. Dessler, P. A. Newman, R. S. Stolarski, A. E. Roche, J. W. Waters, and J. M. Russell III, Development of the Antarctic ozone hole, *J. Geophys. Res.*, *101*, 20,909-20,924, 1996.

Sobel, A. H., R. A. Plumb, and D. W. Waugh, Methods of calculating transport across the polar vortex edge, *J. Atmos. Sci.*, *54*, 2241-2260, 1997.

Solomon, S., R. R. Garcia, F. S. Rowland, and D. J. Wuebbles, On the depletion of Antarctic ozone, *Nature*, *321*, 755-758, 1986.

Stimpfle, R. M., et al., The response of ClO radical concentrations to variations in NO_2 radical concentrations in the lower stratosphere, *Geophys. Res. Lett.*, *21*, 2543-2546, 1994.

Sugita, T., Y. Kondo, H. Nakajima, U. Schmidt, A. Engel, H. Oelhaf, G. Wetzel, M. Koike, and P. A. Newman, Denitrification observed inside the Arctic vortex in February 1995, *J. Geophys. Res.*, *103*, 16,221-16,233, 1998.

Tabazadeh, A., O. B. Toon, S. L. Clegg, and P. Hamill, A new parameterization of H_2SO_4/H_2O aerosol composition: Atmospheric implications, *Geophys. Res. Lett.*, *24*, 1931-1934, 1997.

Tolbert, M. A., M. J. Rossi, R. Malhotra, and D. M. Golden, Reaction of chlorine nitrate with hydrogen chloride and water at Antarctic stratospheric temperatures, *Science*, *238*, 1258-1260, 1987.

Toohey, D. W., L. M. Avallone, L. R. Lait, P. A. Newman, M. R. Schoeberl, D. W. Fahey, E. L. Woodbridge, and J. G. Anderson, The seasonal evolution of reactive chlorine in the northern hemisphere stratosphere, *Science*, *261*, 1134-1136, 1993.

Toon, G. C., C. B. Farmer, L. L. Lowes, P. W. Schaper, J.-F. Blavier, and R. H. Norton, Infrared aircraft measurements of stratospheric composition over Antarctica during September 1987, *J. Geophys. Res.*, *94*, 16,571-16,596, 1989.

Toon, G. C., C. B. Farmer, P. W. Schaper, L. L. Lowes, and R. H. Norton, Composition measurements of the 1989 Arctic winter stratosphere by airborne infrared solar absorption spectroscopy, *J. Geophys. Res.*, *97*, 7939-7961, 1992.

Tuck, A. F., Synoptic and chemical evolution of the Antarctic vortex in late winter and early spring, 1987, *J. Geophys. Res.*, *94*, 11,687-11,737, 1989.

Tuck, A. F., K. K. Kelly, C. R. Webster, M. Loewenstein, R. M. Stimpfle, M. H. Proffitt, and K. R. Chan, Airborne chemistry and dynamics at the edge of the 1994 Antarctic vortex *J. Chem. Soc. Faraday Trans.*, *91*, 3063-3071, 1995a.

Tuck, A. F., C. R. Webster, R. D. May, D. C. Scott, S. J. Hovde, J. W. Elkins, and K. R. Chan, Time and temperature dependences of fractional HCl abundances from airborne data in the southern hemisphere during 1994, *Faraday Discuss.*, *100*, 389-410, 1995b.

Wamsley, P. R., et al., Distribution of halon-1211 in the upper troposphere and lower stratosphere and the 1994 total bromine budget, *J. Geophys. Res.*, *103*, 1513-1526, 1998.

Waugh, D. W., et al., Mixing of polar vortex air with middle latitudes as revealed by tracer-tracer scatterplots, *J. Geophys. Res.*, *102*, 13,119-13,134, 1997.

Webster, C. R., et al., Chlorine chemistry on polar stratospheric cloud particles in the Arctic vortex, *Science*, *261*, 1130-1134, 1993.

Webster, C. R., R. D. May, C. A. Trimble, R. G. Chave, and J. Kendall, Aircraft (ER-2) laser infrared absorption spectrometer (ALIAS) for in situ stratospheric measurements of HCl, N_2O, CH_4, NO_2, and HNO_3, *J. Appl. Opt.*, *33*, 454-472, 1994.

Webster, C. R., et al., Evolution of HCl concentrations in the lower stratosphere from 1991 to 1996 following the eruption of Mt. Pinatubo, *Geophys. Res. Lett.*, *25*, 995-998, 1998.

Woodbridge, et al., Estimates of total organic and inorganic chlorine in the lower stratosphere from in situ and flask measurements during AASE II, *J. Geophys. Res.*, *100*, 3057-3064, 1995.

Zander, R., et al., The 1994 northern midlatitude budget of stratospheric chlorine derived from ATMOS/ATLAS 3 observations, *Geophys. Res. Lett.*, *23*, 2357-2360, 1996.

M. R. Gunson, F. W. Irion, G. L. Manney, J. J. Margitan, R. D. May, D. C. Scott, and C. R. Webster, JPL, 4800 Oak Grove Dr., MS 183-401, Pasadena, CA 91109. (mrg@caesar.jpl.nasa.gov, fwi@caesar.jpl.nasa.gov, manney@mls.jpl.nasa.gov, jjm@mark4sun.jpl.nasa.gov, rmay@alpha1.jpl.nasa.gov, dcscott@alpha1.jpl.nasa.gov, chris.r.webster@jpl.nasa.gov.)

H. A. Michelsen, Sandia National Laboratories, MS 9055, P. O. Box 969, Livermore, CA 94551. (hamiche@ca.sandia.gov.)

J. M. Russell III, Center for Atmospheric Sciences, Hampton Univ., P. O. Box 6075, Hampton, VA 23668. (jmr@cas.hamptonu.edu.)

C. M. Spivakovsky, Dept. of Earth and Planetary Sciences, 29 Oxford St., Harvard Univ., Cambridge, MA 02138. (cms@io.harvard.edu.)

(Received April 12, 1999; revised June 24, 1999;
accepted June 29, 1999)